Marginally trapped surfaces in spherical gravitational collapse

Ayan Chatterjee[*]
Department of Physics and Astronomical Science, Central University of Himachal Pradesh, Dharamshala 176206, India

Amit Ghosh[†]
Theory Division, Saha Institute of Nuclear Physics, 1/AF, Bidhannagar, Kolkata 700064, India

Suresh C. Jaryal[‡]
Department of Physics and Astronomical Science, Central University of Himachal Pradesh, Dharamshala 176206, India

(Received 16 May 2020; accepted 17 August 2020; published 16 September 2020)

This paper deals with a detailed study of horizons during the gravitational collapse of dust and viscous fluids, under the assumptions of spherical symmetry. The formation and time evolution of collapsing shells, spherically symmetric marginally trapped tubes, as well as the event horizon are determined and compared through analytical and numerical techniques. Using different density profiles of matter, we analyze how the nature of these marginally trapped surfaces modify as we change the energy-momentum tensor. These studies reveal that depending on the mass function and the mass profile, it is possible to envisage situations where dynamical horizons, timelike tubes, or isolated horizons arise.

DOI: 10.1103/PhysRevD.102.064048

I. INTRODUCTION

The study of collapse of a self-gravitating isolated system is of great importance in general relativity. Not only is this a problem of physical importance, particularly in understanding the formation of black holes and large-scale structures in the Universe, but also raises fundamental queries related to formation of horizons, spacetime singularities, and the cosmic censorship conjecture [1–6]. The study of gravitational collapse began with the independent work of Datt [7] and Oppenheimer and Snyder [8] (OSD). Although the OSD model is limited to the collapse of a dust cloud of homogeneous density, it shows that within a finite proper time, a spherical ball of matter collapses into a proper radius smaller than its Schwarzschild radius, and eventually, the entire self-gravitating matter collapses into the spacetime singularity. Once the matter crosses the Schwarzschild horizon, no light is able to escape to observers at asymptotic infinity, and hence, the singularity remains hidden to the outside world [1–3]. This is the well-known scenario of black hole formation. Though this model is simple, it is useful for more complicated examples of the collapse of massive astrophysical systems where the matter may have inhomogeneous density, internal pressure, and even possess properties generic to fluids, like viscosity and pressure anisotropies. For example, the well-known Lemaître-Tolman-Bondi (LTB) model of collapse describes the inhomogeneous, pressureless gravitational collapse [9–11]. To understand this large variety of situations, a general formalism to study the dynamical evolution of collapse has been developed. In this method, under various regularity and energy conditions, the initial data are provided in terms of the initial density, pressures, and velocity profiles, and the dynamical evolution is studied using the Einstein equations [4,12,13]. It has been argued that under a large number of fairly regular initial data, both black holes and naked singularities may evolve. A naked singularity is interesting since an observer at infinity may communicate with it. There is much literature on naked singularities, and a comprehensive review and further references on these may be found in [4,14,15]. Another class of singularity which remains visible to observers at infinity is called the shell-crossing singularity [16]. These singularities arise when nearby matter shells create momentary density singularities as a result of which curvature scalars blow up. These are generally *not* regarded as genuine spacetime singularities because they can be removed from the spacetime to extend the manifold. Shell-crossing singularities are gravitationally weak [17], but care must be taken to avoid them.

It is well known that any general relativistic collapse of isolated gravitating matter satisfying regular initial data always results in a spacetime singularity in the form of

[*]ayan.theory@gmail.com
[†]amit.ghosh@saha.ac.in
[‡]suresh.fifthd@gmail.com

geodesic incompleteness if a trapped surface forms, and certain reasonable energy conditions on matter and causal structure of the spacetime hold [1,2]. Additionally, the censorship conjecture rules that the gravitational collapse of matter fields under generic conditions results in the formation of spacetime singularity which remains clothed from the outside world by a horizon. So, if the censorship conjecture is assumed correct, collapse must be followed by a horizon. The most natural description of horizons is the event horizon (EH). However, one fundamental objection against the EH formalism is that it is too global. Indeed, for this definition to work, one must have access to the global development of the spacetime, which may not be possible in all cases. For example, in the numerical simulation of black hole spacetimes, the location of the EH is impossible since the entire evolution of the spacetime cannot be obtained. Such inconsistencies have led to many local definitions of horizon (a detailed overview is in [18–21). The local notions of horizons are based on trapped regions [5]. In these regions, null rays orthogonal to closed 2-surfaces have negative expansion. More precisely, ℓ^a and n^a are, respectively, the outgoing and the ingoing null vectors orthogonal to a two-sphere. The two-sphere is called untrapped, trapped, or marginally trapped depending on whether $\theta_{(\ell)}$ is greater, less, or equal to zero, respectively. Using the marginally trapped surfaces (MTS), one may formulate a definition of horizons. Indeed, several such definitions exist. The notion of the trapping horizon (TH) was introduced in [22] and has found important applications in black hole physics [22,23]. The formulations of isolated horizons (IHs) [24,25] and dynamical horizons (DHs) [26,27], which are closely related to THs, have led to crucial insights into understanding the classical and quantum behavior of black hole horizons [24,25,28]. The DH is a useful tool to describe the smooth dynamical evolution of black hole horizons. The first law (in terms of fluxes) for such a dynamical evolution provides a useful theoretical framework to model black holes evolution [26,27]. Further developments in these directions have been in the development of quasispherical and perturbative approximations of the IH and DH formalisms which are null but admit a well-defined differential version of the first law of black hole mechanics arising due to the influx of (scalar) matter terms [29,30].

The formulation of a marginally trapped tube (MTT) foliated by MTS is a unifying approach to horizons [31]. MTT does not have any particular signature associated with it, and can be null, spacelike, or timelike. Indeed, a null MTT is an IH and hence describes a black hole horizon in equilibrium. When the MTT is spacelike, it is a DH and describes a growing black hole. If the MTT has a timelike signature, it is called a timelike tube, through which matter may cross in either direction. Thus, MTTs provide a unified framework to study time evolution of black holes through different phases. The nature of MTTs and their behavior due to some dust models of collapse like the LTB have been studied in [32] and very recently in [33,34]. Our study provides the evolution of spherical MTTs (which we compare with the collapsing matter shells) for a general class of energy-momentum tensors including viscous effects.

The main motive of this paper is to discuss methods which will be useful to (i) construct spherically symmetric models of spacetime for fluids with general energy-momentum tensors, (ii) study the collapse end state with special emphasis on the formation of horizons, and in particular, track the spherical MTT in each case, and (iii) identify, for the mass profiles considered here, the regions of the parameter space where the spherical MTT evolves as a DH (when matter falls through it), where it might be timelike, and when it becomes an IH. In each example, the exterior geometry will be assumed to be the Schwarzschild spacetime. The study will include brief discussions of the OSD/LTB models and the ones obtained by dropping the assumptions of homogeneity and local anisotropy in the fluid energy-momentum tensor. Interest in these generalities arise because there is a growing attempt in astrophysics to understand the phenomenon of gravitational collapse for different energy-momentum tensors and equations of state [35–39]. As particular examples, the energy-momentum tensors we consider below shall include locally anisotropic fluids, without heat flux, but with shear and bulk viscosity. Local anisotropy in the interior fluid has been argued to arise due to various causes including viscosity or local anisotropic velocity distributions. Such anisotropies would naturally break the conditions of fluid isotropy, and hence, in the presence of viscosity, radial and transverse pressures must be different (in Sec. V, we present a proof). Furthermore, it has been shown that the shear-free condition, particularly in the presence of anisotropy of the pressure and dissipation, leads to instability. These kinds of inhomogeneities and anisotropies in the matter fields are expected to occur quite naturally in the astrophysical systems, particularly during the gravitational collapse, and are expected to play a major role in deciding the spacetime structure. In particular, it has been argued that shear may be responsible for the violation the cosmic censorship leading to a naked singularity in spacetime [4,40]. Thus, it is important that a detailed study of these aspects must be made, and indeed similar kind of models have received attention in the past (see, for example, [41,42]). However, most of the metric configurations are either static or with restricted time dependence. On the other hand, we expect that, in the presence of heat flux, viscosity, or pressure terms, the interior spacetime would be highly dynamical and respond to any fluctuations in the energy-momentum tensor. To incorporate these attributes, in this paper, we relax the assumptions of staticity and generalize these geometries to include time dependence, making these models closer to realistic dynamical systems. More specifically, including anisotropic pressure and the

shear and bulk viscosity terms, we construct explicitly dynamical metric functions.

The paper is arranged as follows. In Sec. II, we briefly set up the definitions and formula for the MTT formalism. In Sec. III, we set up our conventions and the mathematical framework for the Einstein equations and also spell out conditions to ensure that there are no shell-crossing singularities and that the initial spacelike surface does not have any trapped region. Section IV briefly discusses simple collapse models including the marginally bound OSD and the LTB models (we skip the unbounded collapse model since it may be dealt with in a similar fashion). While these models are quite well known (the marginally bounded OSD models are described in [43,44] using the Painleve- Gullstrand coordinates, and the bounded model in [3,37] using the standard coordinates), we present an analytical formula for the (i) collapse of the shells, (ii) time development of the event horizon, and (iii) time development of the spherical MTT (or sometimes called the apparent horizon). These are followed up with examples using specific models of matter profiles to compare with the results well known in the literature. We consider several density profiles and, in each case, determine the evolution of spherically symmetric MTTs and the event horizon. Section V studies models of spacetimes due to viscous fluids. We begin with some generic properties these spacetimes must be endowed with. We show that if the fluid has shear and bulk viscosity, as well as pressure anisotropy, then *generically* the spacetime metric will not be isotropic or have conformal flatness or admit spatially uniform expansion scalar. We also take various density profiles of collapsing matter to show the effects of viscosity on the formation of the spherical MTT. In particular, we show that viscous effects may delay or advance the formation of MTT depending on the coefficients of viscosity. These effects of viscosity are exemplified through various choices of viscosity parameters and mass functions. These studies reveal that it is possible to clearly identify situations where dynamical horizons, timelike tubes, or isolated horizons may arise. We conclude in Sec. VI.

II. HORIZONS AND MARGINALLY TRAPPED TUBES

Let $(\mathcal{M}, g_{ab})$ be a four-dimensional spacetime with signature $(-,+,+,+)$. We shall use the Newmann-Penrose null basis $(\ell^a, n^a, m^a, \bar{m}^a)$, where $\ell \cdot n = -1$, $m \cdot \bar{m} = 1$, while all other dot products vanish. Let Δ be a hypersurface in $\mathcal{M}$. In the following, we shall not restrict the signature of Δ, and hence, it may be spacelike, timelike, or even null. Let us assume that Δ is topologically $S^2 \times \mathbb{R}$. Let ℓ^a and n^a be, respectively, the outgoing and the ingoing vector fields orthogonal to the two-sphere cross sections of Δ. If t^a is a vector field tangential to Δ and normal to foliations, t^a may be written in terms of the ingoing and the outgoing null vector fields as $t^a = \ell^a - Cn^a$ (the sign of C is in accordance with the conventions in [32]). Since $t \cdot t = 2C$, the constant C determines the signature of Δ. The hypersurface Δ will be called a MTT if the following conditions hold true on Δ [31]: (i) $\theta_{(\ell)} = 0$ and (ii) $\theta_{(n)} < 0$.

Several comments are in order regarding these boundary conditions. First, the MTT may be viewed as a unified formalism to describe black hole horizons since Δ has no restriction on its signature. When the MTT is null, it describes black holes in equilibrium (an IH), a growing black hole (a DH) when it is spacelike, or simply a timelike membrane (when Δ is timelike), allowing matter to cross it. The advantage of the MTT formalism is that instead of looking at the evolution of horizons through various phases—dynamical horizons, isolated horizons, and timelike membranes (each phase a multiple number of times)—one may view the horizons as the time evolution of a single MTT. Second, MTT admits a much weaker set of conditions than either the IH or the DH formalism. For example, no restriction on $\pounds_n \theta_{(\ell)}$ is assumed. If $\pounds_n \theta_{(\ell)} < 0$, the MTT is called a future outer trapping horizon [22]. Third, MTTs are foliated by marginally trapped two-spheres. Since t^a is orthogonal to the foliations and tangential to Δ, it generates a foliation-preserving flow so that the following condition holds on Δ:

$$\pounds_t \theta_{(\ell)} \triangleq 0. \tag{1}$$

Fourth, the constant C also measures the evolution of the MTT. To see this, note that if m^a and $\bar{m}^a$ are tangential to the two-sphere cross sections, the area element is given by ${}^2\boldsymbol{\epsilon} = im \wedge \bar{m}$. Under the flow generated by t^a, the area element of MTT evolves as

$$\pounds_t {}^2\boldsymbol{\epsilon} = -C\theta_{(n)} {}^2\boldsymbol{\epsilon}. \tag{2}$$

Naturally, the timelike MTT (for which $C < 0$) contracts and the null MTT ($C = 0$) does not grow, whereas the spacelike MTT (for which $C > 0$) expands. Furthermore, note that no condition on the energy-momentum tensor is assumed on Δ. The Einstein equation $G_{ab} \equiv R_{ab} - (1/2)Rg_{ab} = T_{ab}$ shall be assumed to hold on Δ. We use the units of $c = 1$ and $8\pi G = 1$, or equivalently, we scale the components of the energy-momentum tensor by $8\pi G$.

Several conclusions follow from these conditions. From (1), the constant C is determined by the condition

$$C = \frac{\pounds_\ell \theta_{(\ell)}}{\pounds_n \theta_{(\ell)}}. \tag{3}$$

Using $\theta_{(\ell)} = 0$ and the Einstein equation $G_{ab} = T_{ab}$, we get the following two equations [45]:

$$\pounds_\ell \theta_{(\ell)} = -T_{ab}\ell^a \ell^b, \quad \pounds_n \theta_{(\ell)} = -(\mathcal{R}/2) + T_{ab}\ell^a n^b. \tag{4}$$

Here, $\mathcal{R}$ is the scalar curvature of the round two-sphere and may be rewritten as $\mathcal{R} = (8\pi/\mathcal{A})$, where $\mathcal{A}$ is area of the two-sphere. These equations imply that the constant C which determines the nature of the MTT is given by

$$C = \frac{T_{ab}\ell^a\ell^b}{(4\pi/\mathcal{A}) - T_{ab}\ell^a n^b}. \tag{5}$$

The signature of Δ determined by C is a quantity of utmost importance since it also decides the nature and *stability* of the horizon [46,47]. From the above Eq. (5), this value is controlled by the energy-momentum tensor and area of the marginally trapped surfaces. In the following, we shall use several energy-momentum tensors, including dust models and viscous fluids, and evaluate C in each case. However, as we shall see below, the form of T_{ab} is not the only criterion deciding the signature of the MTT, the mass profile and the equations of collapse are also important factors. Given these complicated constraints, the generic behavior of the MTT is not known for arbitrary black hole evolution. Consider, for example, Vaidya-type black holes evolving under matter fields satisfying dominant energy conditions, the evolution of the MTT is described by the equation $R = 2m(v)$, where v is the advanced Eddington-Finkelstein coordinate. In this case, the MTT is spacelike (more precisely, it is a DH) if $\dot{m}(v) > 0$, where the dot indicates the derivative with respect to the advanced time coordinate [26,27,48]. However, this conclusion does not hold true for any arbitrary collapse scenario. Indeed, even for simple situations like the OSD models of homogeneous dust collapse, a timelike MTT (or a timelike membrane) appears just as the matter cloud reaches the Schwarzschild radius. This timelike membrane, together with the matter cloud, eventually collapses into the singularity at exactly the same time. Examples of trapped surfaces are also discussed in [21,32,43,49–57]. In more realistic LTB inhomogeneous collapse models, the matter cloud and the MTT behave drastically different: The cloud shells reach singularity at different times and the MTT is not purely timelike. For a large number of cases, in which the matter profile is smooth, the MTT begins as a spacelike hypersurface from the center of the cloud and asymptotes to the null event horizons as infall of matter is discontinued. For mass profiles with more complicated functional forms, the time evolution of the MTT shows strange behavior: for example, turning timelike from being spacelike through an intermediate (expanding) null region. These details are studied with a large number of examples as well in the following sections.

III. SPHERICALLY SYMMETRIC COLLAPSE FORMALISM

Let us consider a general spherically symmetric ball of fluid with the line element

$$ds^2 = -e^{2\alpha(r,t)}dt^2 + e^{2\beta(r,t)}dr^2 + R(r,t)^2 d\theta^2 + R(r,t)^2 \sin^2\theta d\phi^2, \tag{6}$$

where $\alpha(r,t)$ and $\beta(r,t)$ are spacetime-dependent functions, θ and ϕ are the angular variables on the sphere, and $R(r,t)$ is the radius of the sphere. This is the standard frame, where the fluid velocity is $u^a = e^{-\alpha}(\partial/\partial t)^a$. This frame allows for a simpler integration of the Einstein equation and the Bianchi identities.

We envisage the solutions of the Einstein equation for the energy-momentum tensor of the spherical ball given by the following form:

$$T_{ab} = (p_t + \rho)u_a u_b + p_t g_{ab} + (p_r - p_t)X_a X_b - 2\eta\sigma_{ab} - \zeta\theta h_{ab}, \tag{7}$$

where η and ζ are the coefficients of shear and bulk viscosity, and X^a is a unit spacelike vector tangential to the spacelike section orthogonal to u^a, respectively, satisfying $X_a X^a = 1$. The quantities σ_{ab}, θ, and h_{ab} are the shear, expansion, and projection tensors and, ρ, p_t, and p_r are the energy density and tangential and radial components of pressure, respectively. The expressions for these quantities are

$$\theta = \nabla_a u^a, \qquad h^a{}_b = (\delta^a{}_b + u^a u_b), \tag{8}$$

$$\sigma^{ab} = \frac{1}{2}(h^{ac}\nabla_c u^b + h^{bc}\nabla_c u^a) - \frac{1}{3}\theta P^{ab}, \qquad X^a = e^{-\beta(r,t)}(\partial/\partial r)^a. \tag{9}$$

Their values for this metric are easily determined to be

$$\theta = e^{-\alpha}(\dot{\beta} + 2\dot{R}/R), \qquad h_{ab} = e^{2\beta(r,t)}dr^2 + R(r,t)^2 d\theta^2 + R(r,t)^2 \sin^2\theta d\phi^2, \tag{10}$$

$$\sigma^1{}_1 = (2/3)(\dot{\beta} - \dot{R}/R)e^{-\alpha}, \qquad \sigma^2{}_2 = \sigma^3{}_3 = (-1/3)(\dot{\beta} - \dot{R}/R)e^{-\alpha}. \tag{11}$$

Let us define a shear scalar $\bar{\sigma}^2 = \sigma_{ab}\sigma^{ab}$, and from the above expressions, we get $\bar{\sigma}^2 = (2/3)e^{-2\alpha}(\dot{\beta} - \dot{R}/R)^2$. For simplification, we shall get rid of the $(2/3)$ factor and redefine $\sigma = e^{-\alpha}(\dot{\beta} - \dot{R}/R)$. The nonzero components of the energy-momentum tensor are given by the following quantities:

$$T^0{}_0 = -\rho, \qquad T^1{}_1 = p_r - \frac{4}{3}\eta\sigma - \theta\zeta, \qquad T^2{}_2 = T^3{}_3 = p_t + \frac{2}{3}\eta\sigma - \theta\zeta. \tag{12}$$

Let us now collect the equations needed to solve our problem of gravitational collapse. Defining the two

functions, $H = e^{-2\alpha(r,t)}\dot{R}^2$ and $G = e^{-2\beta(r,t)}R'^2$, the required equations are

$$\rho = \frac{F'}{R^2 R'}, \tag{13}$$

$$p_r = -\frac{\dot{F}}{R^2\dot{R}} + \frac{4}{3}\eta\sigma + \zeta\theta, \tag{14}$$

$$\alpha' = \frac{2R'}{R}\frac{p_t - p_r + 2\eta\sigma}{\rho + p_r - \frac{4}{3}\eta\sigma - \zeta\theta} - \frac{(p_r - \frac{4}{3}\eta\sigma - \zeta\theta)'}{\rho + p_r - \frac{4}{3}\eta\sigma - \zeta\theta}, \tag{15}$$

$$2\dot{R}' = R'\frac{\dot{G}}{G} + \dot{R}\frac{H'}{H}, \tag{16}$$

$$F = R(1 - G + H). \tag{17}$$

The first two are the G_{00} and the G_{11} equations, the third is the r component of the Bianchi identity, the fourth is the G_{01} component of the Einstein equation, and the fifth is the Misner-Sharp mass function for spherical symmetry. Note from the first Eq. (13) that the density diverges for $R = 0$ as well as $R' = 0$. $R = 0$ implies that the area radius vanishes, which signifies shell focusing singularity at the center of the matter cloud. On the other hand, $R' = 0$ indicates shell-crossing singularities. As is well known, these are gravitationally weak and point to the existence of coordinate singularities. We shall not deal with shell-crossing singularities here.

The number of unknowns in the above equations are three metric variables $\alpha(r,t)$, $\beta(r,t)$, and $R(r,t)$ and the matter variables $p_t, p_r, \rho, \eta\sigma$, and $\zeta\theta$. This gives us the choice of three free functions and the mass function. In the following sections, we shall consider several choices of these free functions and show that these choices, given the regular initial choice of collapse, determine the spacetime uniquely. At the start of the collapse $t_i = 0$, we implicitly consider only those profiles of the matter cloud which satisfy the energy conditions and have regular and smooth energy-momentum tensors. At $t_i = 0$, we use the gauge freedom of the $R(r,t)$ to fix it, so that $R(r,t_i) = r$. In general, this gauge freedom is a scaling of the form $R = ra(r,t)$, where the function $a(r,t)$ will satisfy certain conditions. First, at $t = t_i$, $a(t_i) = 1$, second, at the singularity time t_s, $a(r,t_s) = 0$, and third to maintain the condition of collapse, $\dot{a} < 0$. It immediately follows from Eq. (13) that, at the initial epoch, the density $\rho = F'/r^2$, and hence, the regularity of F at $r = 0$, demands that the r dependence of the mass function take the form $F(r,t) = r^3 m(r,t)$, where $m(r,t)$ is a sufficiently smooth and differentiable function inside the gravitating system. Its t dependence is not determined from Eq. (14) and requires the specification of the p_r and other parameters of the energy-momentum tensor. Also, note that for physical situations, the function $m(r,t)$ must be a smooth and decreasing function of r.

IV. PRESSURELESS COLLAPSE: OSD AND LTB MODELS

For the dust collapse scenario, the viscosity coefficients η and ζ may be taken to be zero. To qualify as dust, the fluid must be pressureless. Furthermore, we impose $p_r = p_t = 0$, which implies that the radial and tangential pressures are equal and vanishing. Equations (13)–(17) simplify to the following equations:

$$F' = \rho R^2 R', \qquad \dot{F} = 0, \tag{18}$$

$$\alpha' = 0, \qquad \frac{\dot{R}'}{R'} = \dot{\beta}. \tag{19}$$

It follows that $R(r,t)$ and the mass function $F(r)$ are related through a constant of integration $k(r)$ [3]:

$$\dot{R}^2 = \frac{F(r)}{R} - k(r). \tag{20}$$

Note that the expression for $\dot{R}$ will have two signatures, +ve for the expanding phase and −ve for the contracting phase. The function $k(r)$ determines the nature of the gravitational collapse. If $k(r) = 0$, we get the marginally bound collapse, where the shells of the matter cloud are assumed to have zero initial velocity at infinity or at the beginning of the collapse, $k(r) > 0$ signifies bounded collapse, where the matter shells have negative initial velocity, whereas $k(r) < 0$ holds for unbounded collapse where matter at the beginning of collapse is assumed to have positive velocity. The metric for this spacetime becomes

$$ds^2 = -dt^2 + \frac{R'(r,t)^2}{1 - k(r)}dr^2 + R(r,t)^2(d\theta^2 + \sin^2\theta d\phi^2). \tag{21}$$

For later convenience, it is useful to rewrite the function $k(r)$ in a scaling form, $k(r) = r^2 K(r)$. The general solution of (20) is

$$t = t_s - \frac{R^{\frac{3}{2}}}{\sqrt{F}}Y\left[\frac{Rk(r)}{F}\right], \tag{22}$$

where t_s is the time for the collapsing shells to reach the central singularity at $R = 0$ and is given by $t_s = r^{3/2}F^{-1/2}Y[rk(r)/F]$. The function $Y(y)$ is given by the following form [3]:

$$Y(y) = \frac{\sin^{-1}\sqrt{y}}{y^{3/2}} - \frac{\sqrt{1-y}}{y}, \qquad 1 \geq y > 0,$$
$$= (2/3), \qquad y = 0,$$
$$= -\frac{\sinh^{-1}\sqrt{-y}}{(-y)^{3/2}} - \frac{\sqrt{1-y}}{y}, \quad 0 > y > -\infty. \tag{23}$$

The quantity C given in (5) determines the signature of the MTT formed during gravitational collapse. For the case of dust, only the density appears in T_{ab}. Using the Einstein equation (13), the equation for C simplifies to

$$C = \frac{2F(r)'}{2R(r,t)' - F(r,t)'}. \tag{24}$$

This formula shall be used in the following sections to determine the nature of the MTT.

A. Homogeneous collapse

For homogeneous collapse, the mass function may be written as $F(r) = mr^3$, where the function $m(r)$ is a constant independent of r. The scaling variable $a(r,t)$ is also reduced to a function of t only, and the function $K(r)$ is taken to be a constant. Incidentally, the values of K here determine the nature of collapse, $K = 0$ indicates the marginally bound collapse, $K = 1$ is for the bounded collapse, and $K = -1$ signifies the unbounded collapse. We shall look into the marginally bound collapse case only since the calculations are similar for the other two cases. For $K = 0$, the solution of the equation of motion (20) is given by Eq. (22):

$$R(r,t) = r\left(1 - \frac{3}{2}\frac{\sqrt{F}}{r^{3/2}}t\right)^{\frac{2}{3}}. \tag{25}$$

Equation (25) gives the time curve for the collapsing shell. Also note that here, $\dot{R} < 0$. The time for the shell to reach singularity, denoted by t_s, follows from Eq. (25) by putting $R = 0$. This gives us $t_s = (2/3\sqrt{m})$. Since m is a constant here, it follows that all shells reach singularity at the same time.

For simplification, we shall shift the singularity time to $t_s = 0$. This essentially shifts the time coordinates linearly without changing any physical content. The motion of the collapsing shell after this shift in time coordinate becomes

$$R(r,t) = [(3/2)\sqrt{F}(-t)]^{\frac{2}{3}}. \tag{26}$$

This equation also gives us the time when the shell reaches the Schwarzschild radius $r = r_H$. Also note that, on the hypersurface, apart from the condition $R = 2M$, one also has the matching conditions at $r = r_H$ given by $F(r_H) = 2M = r_H^3 m$ [see Eq. (A9) in the Appendix]. To find the time t_{2M} for the shell to reach the Schwarzschild radius, we put these conditions in Eq. (26) to get

$$t_{2M} = -\frac{2}{3}F(r_H) = -\frac{4M}{3}. \tag{27}$$

Let us now determine the time development of spherically symmetric MTTs. The equation for the MTT in spherical symmetry is given by the condition $g^{ab}\nabla_a R \nabla_b R = 0$. For the metric being studied here, this implies $R_{\rm AH} = F(r)$. The time curve of the symmetric MTT is obtained from Eq. (26) by using $R = F$ and gives

$$R_{\rm AH}(r) = -\frac{3}{2}t. \tag{28}$$

[1]Naturally, it follows from Eq. (28) that the MTT is formed at $R = 2M$, and shrinks with time and collapses to $R = 0$ at the time of singularity formation $t = t_s$. More precisely, it starts at $R = 2M$ at time t_H, shrinks at a constant rate $\dot{R}_{\rm AH} = -3/2$, and reaches the singularity $r = 0$ at $t = 0$. The collapsing spacetime admits two MTTs. Outside the collapsing region, the MTT matches the $R = 2M$ null surface, whereas inside the collapsing star, the trajectory of the surface follows Eq. (28). Since the MTT outside matches the EH, it is null, whereas, the MTT inside is timelike.

Let us now find the time development of the event horizon. Using the metric, we evaluate the time evolution of the radius along a radial null geodesic. The radial null geodesic of the outgoing photons gives $(dr/dt)_{Null} = 1/R'$. Again, using $dR/dt = [R'(dr/dt)_{Null} + \dot{R}]$, the time evolution of the event horizon reduces to $dR/dt = 1 - \sqrt{F/R}$. Since $R(t)^{3/2} = (3/2)\sqrt{m}r^{3/2}(-t)$ and $F(r) = mr^3$, the previous equation gives

$$\frac{dR}{dt} = 1 + \frac{2}{3}\frac{R}{t}. \tag{29}$$

The solution of this equation gives the event horizon. The general solution of this equation is obtained by integrating with the integrating factor $t^{-2/3}$ and gives

$$R_{\rm EH}(t) = 3t + C'(-t)^{2/3}. \tag{30}$$

The constant C' is fixed as follows: From Eq. (26), the time taken by the shell to reach $R = 2M$ is $t = -4M/3$. Since the event horizon is the last null ray reaching null infinity, we use this condition in Eq. (30) to obtain $C' = 3(9M/2)^{1/3}$. So, from Eq. (30), it follows that the

[1]From Eq. (25), the time curve of the apparent horizon is given by $t_{\rm AH}(r) = (2/3)\sqrt{r^3/F} - (2/3)R_{\rm AH}$. This clearly shows that the AH starts to form at exactly the same time when the shell reaches the Schwarzschild radius, $R = 2M$.

event horizon begins to grow from the nonsingular center just as the collapse process begins. The time of the beginning of the event horizon is obtained from Eq. (30) as follows: Let at $t = t^i_{\rm EH}$, $R_{\rm EH} = 0$. This gives the time of formation of the event horizon $t^i_{\rm EH} = -(9M/2)$. The rate of growth of the event horizon is also obtained from (30): $\dot{R}_{\rm EH} = 3 - 2(9M/2)^{1/3}(-t)^{-1/3}$. This clearly shows that initially, at $t^i_{\rm EH}$, $\dot{R}_{\rm EH} = 1$, whereas, at $t = -4M/3$, just as the shell reaches the Schwarzschild radius (or the null curve of the event horizon reaches $R = 2M$), the event horizon stops growing $\dot{R}_{\rm EH} = 0$ and remains at the Schwarzschild radius. To sum up, the event horizon begins to develop just as the matter shells begin to fall, and then its rate of growth slows down as the rate of fall of matter begins to slow down, ultimately stopping at time $t = -4M/3$ when matter flow stops, and accordingly, it matches with the Schwarzschild null horizon (see the following example).

1. Example

In the following, we consider an example of collapse according to the formalism developed above. The Misner-Sharp mass function is taken to be $F(r) = mr^3$, with $m = (1/2)$. The $t - R(r,t)$ graph for the collapse is given below in Fig. 1. We have taken care to exclude shell-crossing singularities and have ensured that there are no trapped surfaces on the initial slice. Several points need to be noticed. First, all the shells collapse into the singularity at the same time at $t = 0.94$. Second, the shell which begins at $R(r,t) = 1$ reaches its Schwarzschild radius at time $t = 0.61$, and exactly at that instant, the event horizon (or the last null ray) beginning at the center of the cloud also reaches that spacetime point. Third, the spherically symmetric MTT also forms at that point and eventually collapses into singularity, along with the matter cloud. Further, the signature of C establishes that the MTT is timelike.

B. Inhomogeneous collapse

For the inhomogeneous collapse, $\alpha = \alpha(t)$ in the metric and may again be absorbed through the redefinition of the time coordinates; see Eq. (18). The mass function still remains a function of r only and is taken to be of the form $F(r,t) = r^3 m(r)$ and the metric function is given by $k(r) = K(r)r^2$.

1. Marginally bounded collapse

The marginally bounded collapse corresponds to $K = 0$. The metric is given by

$$ds^2 = -dt^2 + R'^2(r,t)dr^2 + R^2(r,t)(d\theta^2 + \sin^2\theta d\phi^2), \tag{31}$$

where $R(r,t)$ is the radius of the shell. The equation of motion of the shell is given by $\dot{R}^2 = F(r)/R$. The solution of the equation of motion is given by the following form:

$$t = (2/3)\left[\sqrt{r^3/F} - \sqrt{R(r,t)^3/F}\right], \tag{32}$$

where the radius of the shell at the beginning of the collapse at $t_i = 0$ is $R(r,t_i) = r$. The shells will be labeled by the value of the radius it assumes at the initial time $t = 0$. For example, for the shell being studied above, it shall be labeled by the coordinate r. For this shell, the time taken for it to reach the singularity is $t_s = (2/3)r^{3/2}/\sqrt{F}$. Note that since $F(r)$ is inhomogeneous, all shells do not reach the singularity at the same time. The equation of motion given above for the shell may naturally be rewritten as

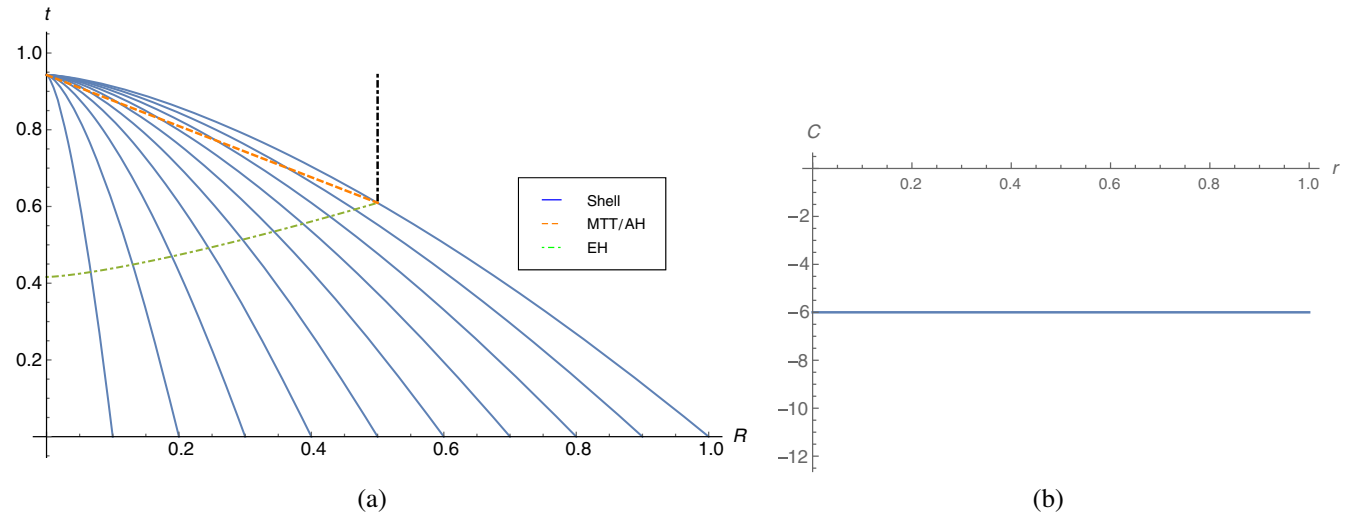

(a) (b)

FIG. 1. (a) gives the plot of $R(r,t)$ vs t for the mass profile discussed above. The MTT is timelike and is also confirmed through the negative value of C in the graph of $C - r$ in (b).

$t = t_s - (2/3)\sqrt{R(r,t)^3/F}$. If the time coordinate is shifted to make $t_s = 0$, the time for the shell to reach $R = 2M$ becomes $t_{2M} = (-4M/3)$.

The equation of the spherically symmetric MTS is obtained by using the condition $R(r,t) = F(r)$ giving the equation for the MTT to be $R_{\rm AH}(r,t) = -(3/2)t$. So, the MTT begins at $R = 2M$, shrinks at a constant rate of $\dot{R}_{\rm AH} = -(3/2)$, and goes to zero at the same time when the singularity forms. The apparent horizon which is outside the shell matches the Schwarzschild null event horizon. Note that the slope of the $R_{\rm AH}(r,t) - t$ graph is negative. However, this does not mean that the MTT is timelike. In the examples that follow, we shall show that even if the MTT behaves as a timelike curve in the $R(r,t) - t$ graph, it is the constant C which fixes the signature of the MTT [32,46].

Let us now look at the formation of the event horizon, for which we need to look at the radial null geodesic given by the curve $R[r, t_n(r)]$. The event horizon shall be obtained by tracing the last radial null geodesic reaching null infinity. Using techniques developed in the previous subsections, the equation for the event horizon is given by $R_{\rm EH} = 3t + 3(9M/2)^{1/3}(-t)^{2/3}$. Note that just as in the case for homogeneous collapse, the event horizon begins just as the matter shells begin to fall, growing slowly to smoothly match the Schwarzschild horizon at $R = 2M$ at $t = -4M/3$. At that time, the rate of growth of $R_{\rm EH}$ vanishes, and for $t \geq -4M/3$, the event horizon is the null Schwarzschild horizon of radius $2M$.

2. Examples

Here, we consider two examples, with the densities having the following forms:

$$\rho_1(r) = (3M/2500)(10 - r)\Theta(10 - r),$$
$$\rho_2(r) = (3M/40\sqrt{10})(10 - r^2)\Theta(10 - r^2), \qquad (33)$$

where $\Theta(x)$ denotes the Heaviside theta function. The factors have been chosen to get the isolated horizon at $R(r,t) = 2$, and the corresponding masses have been normalized with the choice $M = 1$. In each case, the spherically symmetric MTTs are spacelike, as indicated by the values of C. Again, there are no shell-crossing singularities and no trapped surfaces on the initial slice. The $R - t$ plots, however, are intricate in these two cases and are markedly different (see Figs. 2 and 3). We give these two cases since they show the nontrivial ways in which the MTTs cross the foliation. For the density profile corresponding to ρ_1, the MTTs are spacelike. As seen from the $R(r,t) - t$ graph, the MTT forms out of the central singularity, evolves in a spacelike manner, and approaches the isolated horizon phase at $R = 2$. Although it may seem from these graphs that timelike membranes arise here, the graphs of C verify that it is not so. This bending of graphs only indicates that the MTTs cross the foliation in intricate ways [32,46].

3. Bounded collapse

For the case of bounded collapse $k(r) > 0$, the parametric solutions are given by

$$R(r,t) = \frac{F(r)}{k(r)}\cos^2(\eta/2) = r\cos^2(\eta/2), \qquad (34)$$

$$t = \frac{F(r)}{2k(r)^{3/2}}(\eta + \sin\eta) = \frac{r^{3/2}}{\sqrt{F}}(\eta + \sin\eta), \qquad (35)$$

where we assume the function $k(r)$ to be of the form $k(r) = F(r,t)/r$, with $F(r,t) = m(r)r^3$. The collapse of the cloud begins at $\eta = 0$, where $t = t_i = 0$ and $R(r,t_i) = r$ and reaches the singularity at $\eta = \pi$ where $R = 0$. The time for collapsing shells labeled by r to reach the central singularity $R = 0$ is $t_s = \pi/2m(r)^{1/2}$. So, shells with different initial radius reach the central singularity at different times. From Eq. (34), the proper time for the shell to reach the Schwarzschild radius $R = 2M$ is given by $\eta_{2M} = 2\cos^{-1}(2M/r)^{1/2}$.

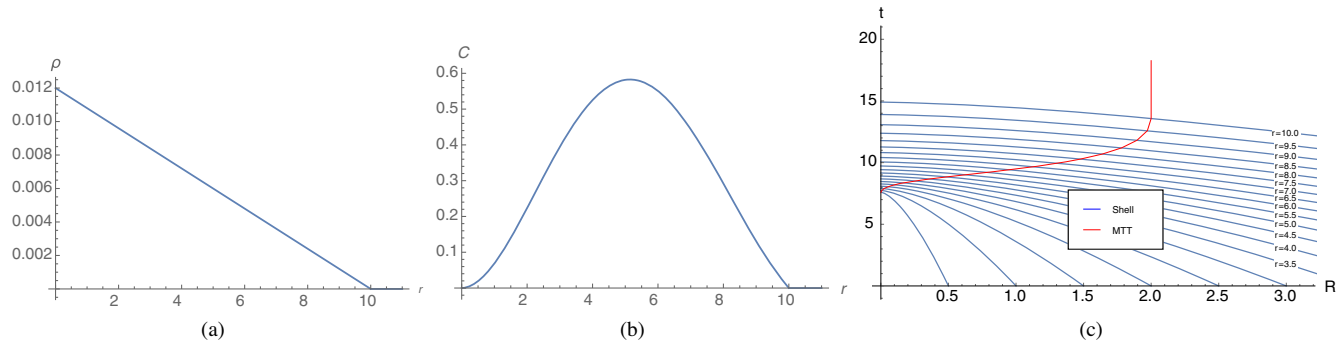

(a) (b) (c)

FIG. 2. The graphs show the (a) density distribution ρ_1, (b) values of C, and (c) formation of the MTT along with the shells. The MTT begins from the center of the cloud. The straight lines of the MTT in (c) after the shell $r = 10$ has fallen represents the isolated horizon phase. The value of C indicates that the spherical MTT is spacelike.

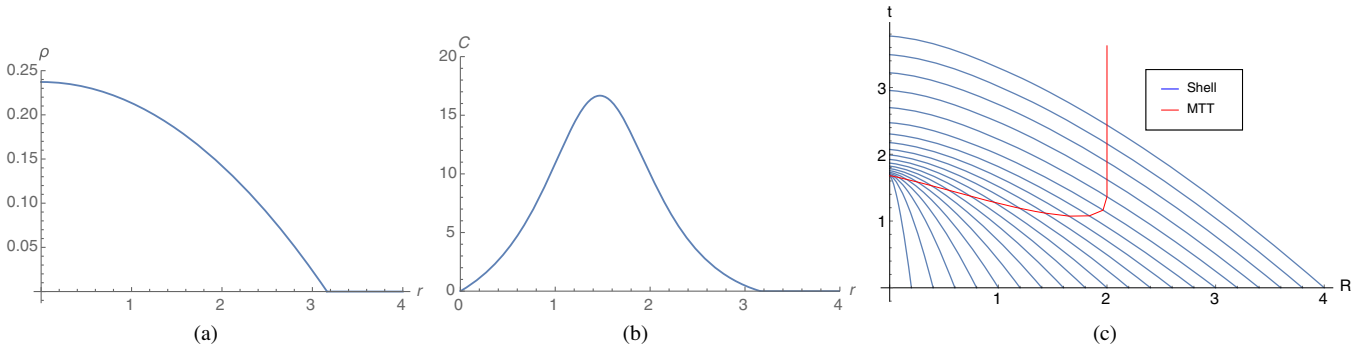

FIG. 3. The graphs show the (a) density distribution ρ_2, (b) values of C, and (c) formation of the MTT along with the shells. Note that the MTT seems to begin at $r = 2.6$ and then bifurcates in a timelike manner to the singularity, while another part proceeds toward the isolated horizon. However, since the signature of C is always positive, the behavior of the MTT must be similar to Fig. 2. The timelike feature is due to nontrivial intersection with the foliation [32,46].

Let us now locate the spherically symmetric MTTs. From Eqs. (34) and (35), a simple calculation gives a complicated-looking expression relating the change of the shell radius of the MTS with respect to proper time η,

$$\frac{dr_{\rm AH}}{d\eta} = -\frac{(\sin\eta)/2 + (1-k/k)^{1/2}\cos^2(\eta/2)}{D}, \tag{36}$$

where the denominator D is given by the following form:

$$D = (kF'/F) - [(F'/F) - (k'/k)]\cos^2\eta/2 + [(1-k)/4k]^{1/2}(F'/F - 3k'/2k)[\eta + \sin(\eta)]. \tag{37}$$

Using the solutions of (36) into (34) and (35) gives the equation of spherical trapped surfaces. Also, from Eq. (35), at this same time, the MTT should be at $R = 2M = F$. On the other hand, the equation for the evolution of the event horizon is given by

$$\frac{dr_{\rm EH}}{d\eta} = -\frac{(\sin\eta/2) + (1-k/k)^{1/2}\cos^2(\eta/2)}{\bar{D}}, \tag{38}$$

where the denominator $\bar{D}$ is given by the following form:

$$\bar{D} = [(F'/F) - (k'/k)]\cos^2\eta/2 - [(1-k)/4k]^{1/2}(F'/F - 3k'/2k)[\eta + \sin(\eta)]. \tag{39}$$

We have considered (r_H, η_{2M}) to be the point where the outer event horizon forms. Thus, the equation of the event horizon is given by

$$R_{\rm EH} = r_{\rm EH}\cos\left[\frac{\eta}{2}\right]^2. \tag{40}$$

We have all the required equations to study the LTB collapsing shells (34), apparent horizon [from (34)], and event horizon (40). As a simple example, let us consider the matching of the interior to the exterior at the hypersurface when $\chi_H = \pi/3$, $r_H = 0.866$, and $m(r) = (n_0 + rn_1)$, such that the point where the even horizon formed is $(\eta_{2M}, R_{2M}) = (2.1399, 2.0)$. Thus, all the three curves, that of collapsing shell, the apparent horizon, and the event horizon should meet at $R = 2.0$ when $\eta_{2M} = 2.1399$ for $n_0 = 1/11$ and $n_1 = 1/4$.

4. Examples

(i) Let us consider a Gaussian profile with the density given by the following form [32]:

$$\rho(r) = \frac{m_0}{\pi^{3/2}r_0^3}\exp(-r^2/r_0^2), \tag{41}$$

where m_0 is the total mass of the matter cloud, and r_0 is a parameter which indicates the distance where the density of the cloud decreases to $[\rho(0)/e]$. In our example, we have chosen $r_0 = 100m_0$. As usual, the symmetric MTT begins from the central singularity and develops as a dynamical horizon until approximately $r = 200$, where it begins to resemble an isolated horizon (see Fig. 4). This may also be confirmed from the fact that the density at $r = 200$ is almost negligible. However, since the Gaussian profile almost disappears at $r = 380$, the $R = 2$ is also reached at that value of the shell coordinates.

(ii) Let us consider another density profile with the following form:

$$\rho(r) = \frac{m_0}{8\pi r_0^3}\exp(-r/r_0), \tag{42}$$

where m_0 is the total mass of the matter cloud, and r_0 is a parameter which indicates the distance where the density of the cloud decreases to $[\rho(0)/e]$. The spherically symmetric MTT begins from the central singularity and develops as a dynamical horizon until approximately $r = 70$, where it begins to resemble an isolated horizon. This may also be

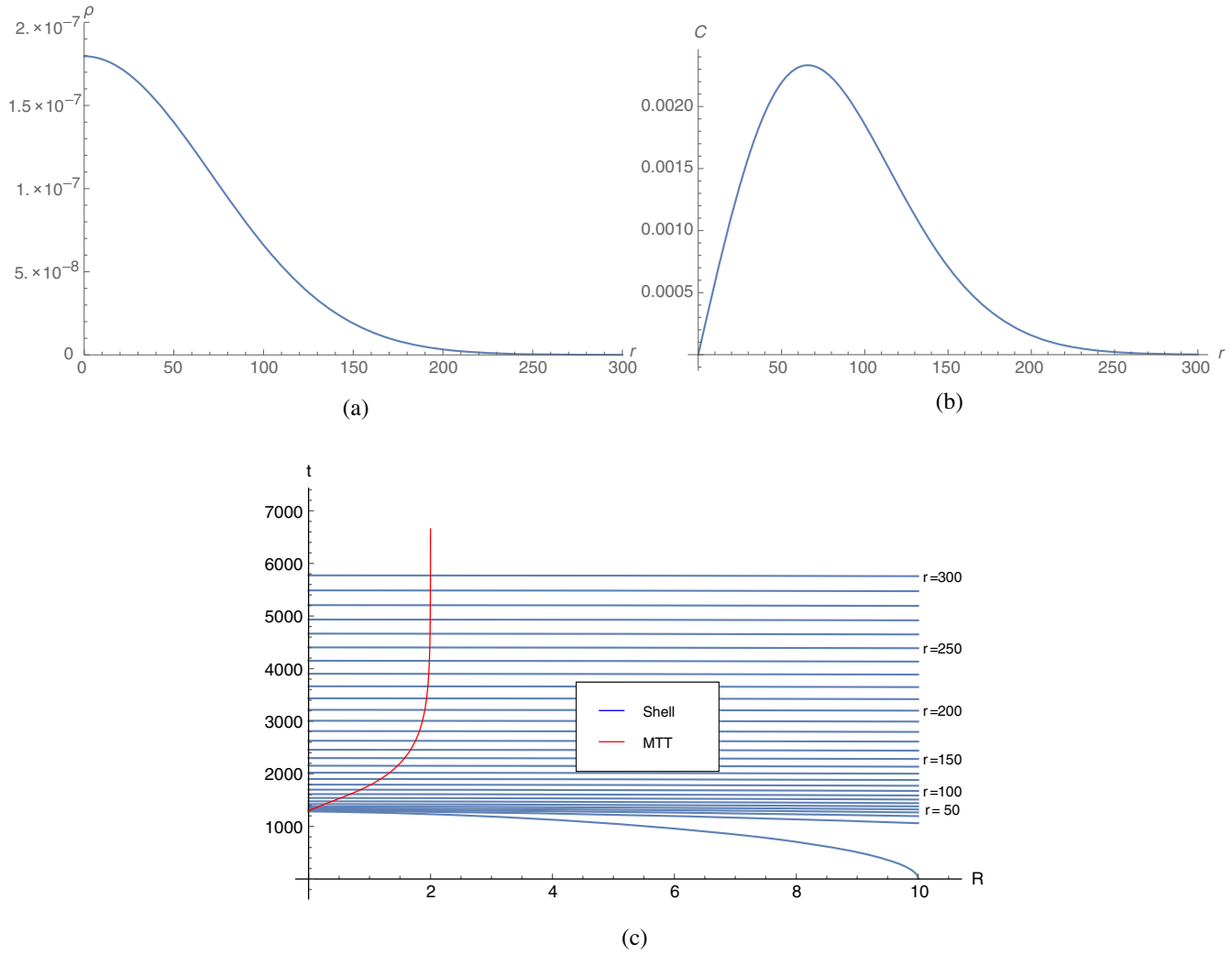

FIG. 4. The graphs show the (a) density distribution, (b) values of C, and (c) formation of the MTT along with the shells. The MTT begins from the center of the cloud. The straight lines of the MTT in (c) after the shell $r = 250$ represent the isolated horizon phase.

confirmed from the fact that the density at $r = 70$ is almost negligible. However, since the Gaussian profile almost disappears at $r = 100$, the $R = 2$ is also reached at that value of the shell coordinates. This may be seen from Fig. 5.

(iii) Two shells falling consecutively on a black hole: Let us assume that a black hole of mass M exists, upon which a density profile of the following form falls:

$$\rho(r) = \frac{8(m_0/r_0^3)[(r/r_0) - \varsigma]^2}{[2\varsigma + (3 + 2\varsigma^2)\sqrt{\pi}e^{\varsigma^2}\{1 + \mathrm{Erf}(\varsigma)\}]} \times \exp[(2r/r_0)\varsigma - (r/r_0)^2], \tag{43}$$

where $m_0 = M/2$ is the mass of the shell, and $2r_0$ is the width of each shell. If we assume that the initial black hole has the Schwarzschild radius given by $\bar{r} = 2M$, then the mass for each shell of radius $r(r > \bar{r})$ is then $m(r) = M + \int_{\bar{r}}^{r} \rho(\hat{r})\hat{r}^2 d\hat{r}$. The quantity σ is a parameter which denotes the position where the density vanishes. Here, we have used $M = 1$, $r_0 = 10$, and $\varsigma = 10$. At around $r = 65$, the MTT starts to grow in a spacelike fashion and reaches approximately $R = 2.4$ at approximately $t = 1014$ when the $r = 100$th shell falls. Note that at this time, the C vanishes making the MTT null. This is expected since the density of the shell goes to zero here (see Fig. 6). Again, just as the next shell starts to fall, the MTT again begins to evolve in a spacelike fashion to reach $R = 3$ at $t = 1500$ when the shell denoted by $r = 140$ has fallen in.

V. SPACETIMES ADMITTING VISCOUS MATTER FIELDS

In this section, we shall consider spacetimes due to collapse of matter whose energy-momentum tensor contains viscous matter fields. The Einstein equations are

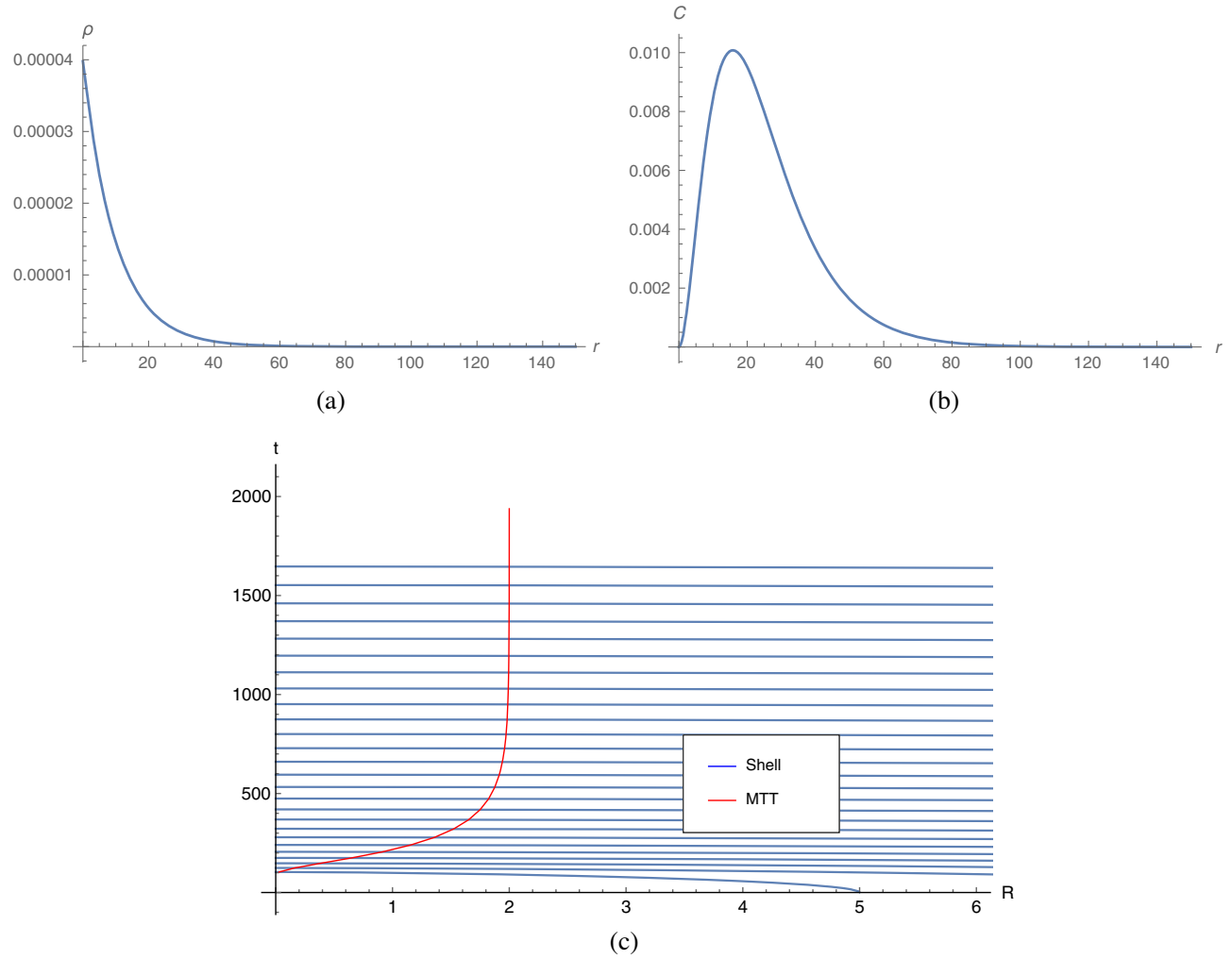

FIG. 5. The graphs show the (a) density distribution, (b) values of C, and (c) formation of the MTT along with the shells. The MTT begins from the center of the cloud. The straight lines of the MTT in (c) represent the isolated horizon phase.

Eqs. (13)–(17). For simplification, we shall also assume some form of equation-of-state-type relations between some geometric scalar quantities and the density. First, note that one may envisage some exact relations involving the Newman-Penrose scalar ψ_2 and the Misner-Sharp mass function [58,59]. The quantity ψ_2 for this spacetime is given by

$$\begin{aligned}\psi_2 = \frac{e^{-2\beta}}{6}[&\alpha'' + \alpha'^2 - \alpha'\beta' + R'^2/R^2 - R''/R \\ &+ (R'\beta')/R - (R'\alpha')/R] - \frac{1}{6R^2} \\ &- \frac{e^{-2\alpha}}{6}[\ddot{\beta} + \dot{\beta}^2 - \dot{\alpha}\dot{\beta} + \dot{R}^2/R^2 - \ddot{R}/R \\ &- (\dot{R}\dot{\psi})/R + (\dot{R}\dot{\alpha})/R]. \end{aligned} \tag{44}$$

Using the Einstein equations, Eq. (44) can be written in terms of the mass function $F(r,t)$ in Eq. (17):

$$F(r,t) = (\rho + \bar{p}_t - \bar{p}_r + 2\eta\sigma)(R^3/3) - (\psi_2/2)R^3, \tag{45}$$

where $\bar{p}_r = (p_r - \zeta\theta)$ and $\bar{p}_t = (p_t - \zeta\theta)$. The quantity $\mathcal{F}(r,t) = -\psi_2 R^3$ has a similar stature as the mass function [58]. Its derivatives are given by

$$\begin{aligned}\dot{\mathcal{F}} = &-(1/6)[R^3\{\rho + \bar{p}_t + (2/3)\eta\sigma\}]_{,t} \\ &- (R^3/6)[\bar{p}_r - (4/3)\eta\sigma]_{,t}, \end{aligned} \tag{46}$$

$$\mathcal{F}' = -(1/6)R^3\rho' - (1/6)[R^3(\bar{p}_t - \bar{p}_r + 2\eta\sigma)]'. \tag{47}$$

These two equations may be combined to extract an expression for the time derivative of the density $\dot{\rho}$:

$$\dot{\rho}e^{-\alpha} + [\rho + \bar{p}_r - (4/3)\eta\sigma](\Theta - \sigma) = 0. \tag{48}$$

On the other hand, the expression for $\dot{\rho}$ and p_r' may also be derived from the Bianchi identities:

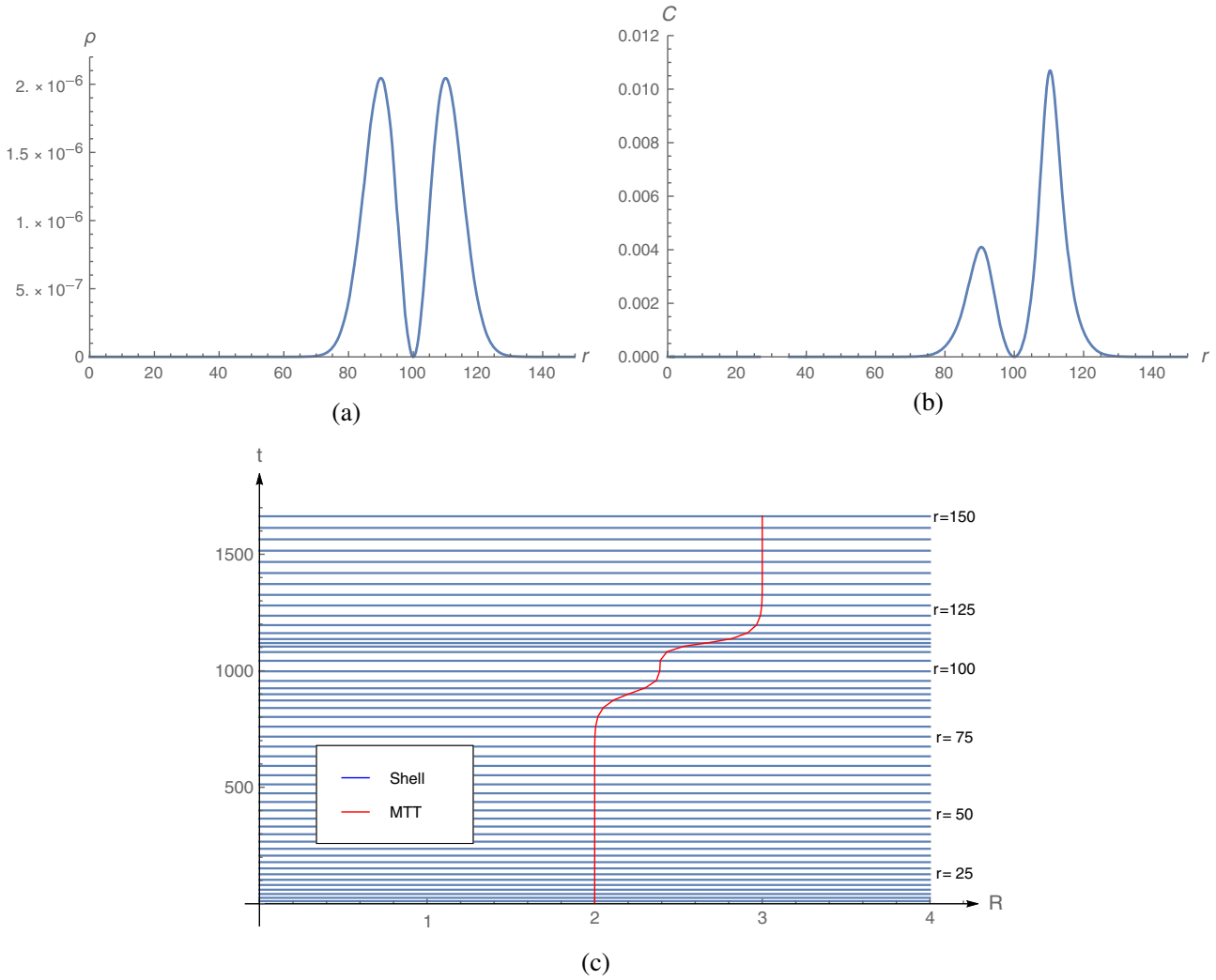

FIG. 6. The graphs show the (a) density distribution, (b) values of C, and (c) formation of the MTT along with the shells which fall consecutively on a black hole. The MTT begins from $R = 2$, where the previous EH is situated. The straight lines of the MTT in (c) represent the isolated horizon phase.

$$\dot{\rho} = -\dot{\beta}[\rho + \bar{p}_r - (4/3)\eta\sigma] - (2\dot{R}/R)[\rho + \bar{p}_t + (2/3)\eta\sigma], \tag{49}$$

$$p_r' = \{(4/3)\eta\sigma\}' + (2R'/R)(\bar{p}_t - \bar{p}_r + 2\eta\sigma) - \alpha'\{\rho + \bar{p}_r - (4/3)\eta\sigma\}. \tag{50}$$

Using the Bianchi identity (49) into Eq. (48), we have a relation involving the matter variables and the geometric variables given by

$$(\rho + \bar{p}_r) = \frac{8}{3}\eta\sigma - \frac{4}{3}\eta\theta + e^{-\alpha}\frac{2\dot{R}}{R\sigma}(\bar{p}_t - \bar{p}_r). \tag{51}$$

This equation gives some crucial input regarding the pressure anisotropy $(\bar{p}_t - \bar{p}_r)$ and its relation to the shear scalar σ. The pressure anisotropy must be interpreted as the generator of the shear scalar and hence must be proportional to it. Indeed, using Eq. (51) in (49), we have

$$\dot{\rho} = \frac{6\dot{R}^2}{R^2}e^{-\alpha}\left[2\eta + \frac{\bar{p}_t - \bar{p}_r}{\sigma}\right], \tag{52}$$

which makes our claim, that pressure anisotropy must lead to shear, explicit. We shall show below that the claim still holds even if we assume the matter density to be spatially uniform throughout the collapsing cloud. We must point out that such an assumption is not contradictory to the presence of shear or pressure anisotropy. We shall elaborate on this issue below as well as in the following sections when we take specific examples. To show this, we first derive another expression for the time change of density which involves the radial pressure only. If the density is uniform, simple integration of Eqs. (47) implies that

$\mathcal{F}(r,t) = -(R^3/6)(\bar{p}_t - \bar{p}_r + 2\eta\sigma)$. Using this in (46), we have

$$\dot{\rho} = -(3\dot{R}/R)[\rho + \bar{p}_r - (4/3)\eta\sigma]. \tag{53}$$

Now, let us rewrite the Binachi identity (49) using Eqs. (10), which gives us

$$(\rho + \bar{p}_r)\theta = -\dot{\rho}e^{-\alpha} - \frac{2\dot{R}}{R}(\bar{p}_t - \bar{p}_r)e^{-\alpha} + \frac{4}{3}\eta\sigma^2, \tag{54}$$

which may also be written in the following form, equivalent to (52):

$$\dot{\rho}e^{-\alpha} = [(4/3)\eta\sigma^2 - (\rho + \bar{p}_r)\Theta]\left[1 - \frac{(2/3)(\bar{p}_t - \bar{p}_r)}{\rho + \bar{p}_r - (4/3)\eta\sigma}\right]^{-1}. \tag{55}$$

The radial derivative of Eq. (54) along with (55) gives the following equation:

$$(\rho + \bar{p}_r)\theta' + (\rho + \bar{p}_r)'\theta = (\dot{\rho}e^{-\alpha})'\left[1 + \frac{(2/3)(\bar{p}_t - \bar{p}_r)}{\rho + \bar{p}_r - (4/3)\eta\sigma}\right] + [(4/3)\eta\sigma^2]' - \dot{\rho}e^{-\alpha}\left[\frac{(2/3)(\bar{p}_t - \bar{p}_r)}{(\rho + \bar{p}_r - (4/3)\eta\sigma)}\right]', \tag{56}$$

which along with the radial part of Bianchi identity (50) gives the following elaborate form

$$\begin{aligned}(\rho + \bar{p}_r)\theta' = &-[(4/3)\eta\sigma' - (4/3)\eta\sigma\alpha' + (2R'/R)(\bar{p}_t - \bar{p}_r + 2\eta\sigma)]\theta \\ &+ \left[\frac{(2/3)}{(\rho + \bar{p}_r - (4/3)\eta\sigma) - \frac{2}{3}(\bar{p}_t - \bar{p}_r)}\right]\left[\alpha'(\rho + \bar{p}_r)\{2\eta\sigma^2 - \bar{p}_t\theta(\bar{p}_t - \bar{p}_r)\}\right. \\ &+ \{(\rho + \bar{p}_r)\Theta + (4/3)\eta\sigma^2\}\left\{(\bar{p}_t - \bar{p}_r)' - \frac{2(\bar{p}_t - \bar{p}_r)^2}{(\rho + \bar{p}_r - 4/3\cdot\eta\sigma)}\right. \\ &\left.\left. - \frac{4\eta\sigma(\bar{p}_t - \bar{p}_r)}{(\rho + \bar{p}_r - 4/3\cdot\eta\sigma)}\right\} - 8/3\cdot\alpha'\eta^2\sigma^3\right] + \{(4/3)\eta\sigma^2\}'.\end{aligned} \tag{57}$$

Several results follow directly from Eq. (57). Let the pressure anisotropy $(p_t - p_r)$ and the viscosity parameters η and ζ vanish. If we write $p_r = p_t \equiv p$, then the above equation reduces to

$$(\rho + p)\theta' = 0. \tag{58}$$

This implies that, during the gravitational collapse of uniform density perfect fluid having irrotational motion, the expansion scalar must remain spatially uniform. Furthermore, the spacetime must be isotropic as well as conformally flat [59–61]. These results hold true even if the spacetime has bulk viscosity but negligible shear viscosity [59]. However, if the fluid is dissipative, with nonvanishing shear viscosity, these results do not hold and expansion becomes a scalar function. The situation however alters significantly if the pressure anisotropy arising through $(p_t - p_r)$ is also taken into account. As may be seen from Eq. (57), these anisotropies are in the same footing as the shear terms. Indeed, then one may envisage situations where the quantities arising from the dissipative forces, like the shear and bulk viscosity, cancel those due to anisotropy, leading to a spatially uniform expansion scalar, just like for perfect fluids. Although that situation would be highly fine-tuned, it is not unlikely. To summarize, we have shown that if the fluid has shear and bulk viscosity, as well as pressure anisotropy, then *generically* the spacetime will not admit isotropy, conformal flatness, or a spatially uniform expansion scalar.

This brings into question whether the local anisotropy of fluids may be identified as the source of viscous effects. Given the form of these quantities in (51), (52), and (57), this expectation holds ground. In the following, we shall assume that a relation of this kind does exist, and to give form to this expectation, we assume a simple linear relation among these quantities, like $(p_t - p_r) \propto \sigma$. To put it in better perspective, they will be related to the density function through the following constraints: $p_t = k_t\rho$, $\sigma = k_\sigma\rho$, and $\theta = k_\theta\rho$. The values of the constants k_t, k_σ, and k_θ shall be chosen to observe the effects of $(p_t - p_r)$ on the time development of horizons.

A. Time-independent mass function

To study realistic collapse phenomena, the pressure and viscosity contributions to the energy-momentum tensor of the collapsing cloud must be included. To begin with, let us assume that the collapsing cloud has a certain fixed radial pressure given by $p_r = (4/3)\eta\sigma + \zeta\theta$. This particular combination is chosen so that the viscosity terms in the equation of motion cancel the effects of radial pressure during the collapse. This choice also keeps continuity with the study of pressureless collapse carried out in the previous sections. However, to retain the physical

importance of the model, we shall keep the combination $[p_t + (2/3)\eta\sigma - \zeta\theta]$ to be nonzero. This particular term includes the tangential part of the pressure along with certain viscosity terms. The reason for this choice is only mathematical simplicity. Also, as we shall see, this choice gives us a time-independent Misner-Sharp mass function.

The set of Einstein equations for the gravitational collapse of matter satisfying these conditions is given by

$$F' = \rho R' R^2, \qquad \dot{F} = -(R^2\dot{R})\left(p_r + \frac{4}{3}\eta\sigma - \zeta\theta\right) = 0, \tag{59}$$

$$\alpha' = (2R'/\rho R)[p_t + (2/3)\eta\sigma - \zeta\theta], \tag{60}$$

$$(\dot{G}/G) = 2\alpha'(\dot{R}/R'), \tag{61}$$

$$F(r,t) = R(r,t)(1 - G + H), \tag{62}$$

where $H(r,t) = e^{-2\alpha(r,t)}\dot{R}^2$ and $G(r,t) = e^{-2\beta(r,t)}R'^2$. The number of unknowns to be determined here are more than the independent Einstein equations (59)–(62); we close the system with the constraints $p_t = k_t\rho$, $\sigma = k_\sigma\rho$, and $\theta = k_\theta\rho$ given above. Using these equations of state, the solutions of the Einstein equations (60) and (61) become

$$\exp(2\alpha) = R^{4a_1}, \qquad \exp(2\beta) = \frac{R'^2}{b(r)R^{4a_1}}, \tag{63}$$

where we have introduced the constants $a_1 = k_t + (2/3)\eta k_\sigma - \zeta k_\theta$. Using these redefinitions, the line element (6) may be rewritten as

$$ds^2 = -R^{4a_1}dt^2 + \frac{R'^2}{b(r)R^{4a_1}}dr^2 + R(r,t)^2 d\theta^2 + R(r,t)^2\sin^2\theta d\phi^2. \tag{64}$$

The equation of motion (62) is also simplified to have the following form:

$$\dot{R} = -R^{2a}\left[\frac{F(r)}{R} - 1 + b(r)R^{4a_1}\right]^{1/2}. \tag{65}$$

To study evolution of the horizon and the outgoing null geodesics (and the event horizon), and to simplify the solutions of the equation of motion (62), we choose the parameter to be $a_1 = -(1/4)$. This choice simplifies the solution of the equation of motion (62), and the time curve of the collapsing shell is given by

$$dt = -\frac{RdR}{[F(r) + b(r) - R(r,t)]^{1/2}}. \tag{66}$$

To solve the integral, we choose a parametric form to relate the functions $R(r,t)$, $F(r)$, and $b(r)$. A particular simple choice is $R = (F/b)\cos^2(\eta/2)$. Using this form, the equation of collapse simplifies, and the time curve is obtained from the equation

$$dt = \left(\frac{F^2}{2b^2}\right)\frac{\sin\eta\cos^2(\eta/2)}{[F + b - (F/b)\cos^2(\eta/2)]^{1/2}}d\eta. \tag{67}$$

The solution of this equation is the time curve of the collapsing shell and is given by

$$t = \frac{4}{3}[F + b - (F/b)\cos^2(\eta/2)]^{1/2} \times [F + b + (F/2b)\cos^2(\eta/2)] - (4/3)\{F + b - (F/b)\}^{1/2}[F + b + (F/2b)]. \tag{68}$$

The boundary conditions are chosen such that the collapse begins at $\eta = 0$ and reaches the central singularity at $\eta = \pi$. At the beginning of the collapse $\eta = 0$, we have $R(t_i, r) = [F(r)/b(r)]$ with $t_i = 0$. At the end state of the collapse process when $\eta = \pi$, we naturally have $R = 0$. Note that the time of formation of central singularity, or the time the shell reaches singularity, is also obtained from the above equation:

$$t_s = \frac{4}{3}[(F + b)^{\frac{3}{2}} - \{F + b - (F/b)\}^{1/2}\{F + b + (F/2b)\}]. \tag{69}$$

From these equations, it is also possible to track the formation of spherical MTTs and determine the exact time when the shell reaches its Schwarzschild radius.

The dynamics of the marginally trapped surfaces (whether they are timelike, spacelike, or null) depends upon the sign of the expansion parameter C defined in Eq. (5). We take the timelike vector field to be $u^\mu = \chi l^\mu + (2\chi)^{-1}n^\nu$ and the spacelike vector field to be $x^\mu = \chi l^\mu - (2\chi)^{-1}n^\nu$:

$$T_{\mu\nu}l^\mu l^\nu = (1/4\chi)[\rho + p_t - (4/3)\eta\sigma - \zeta\theta + (p_t - p_r)], \tag{70}$$

$$T_{\mu\nu}l^\mu n^\nu = (1/2)[\rho - (p_t - (4/3)\eta\sigma - \zeta\theta + (p_t - p_r))]. \tag{71}$$

Using $p_r = (4/3)\eta\sigma + \zeta\theta$, the equations lead to the following form of C:

$$C = (1/2\chi)\left[\frac{\rho + 2\{p_t - (4/3)\eta\sigma - \zeta\theta\}}{4\pi/\mathcal{A} - (1/2)[\rho - 2\{p_t - (4/3)\eta\sigma - \zeta\theta\}]}\right]. \tag{72}$$

1. Examples

(i) Let us consider a Gaussian density profile as before given by $\rho(r) = [m_0/\pi^{3/2}r_0^3]\exp(-r^2/r_0^2)$, where m_0 is the total mass of the matter cloud, and r_0 is a parameter which indicates the distance where the density of the cloud decreases to $[\rho(0)/e]$. Just as before, we choose $r_0 = 100m_0$. Here also, the spherical MTT begins from the central singularity and develops as a dynamical horizon until it approaches the isolated horizon at approximately $r = 200$. This may also be confirmed from the fact that the density at $r = 200$ is almost negligible. The density profile almost disappears at $r = 380$, and beginning at that value of the shell coordinate, the MTT remains at $R = 2$. The nature of the formation of singularity is identical to the LTB case discussed in the previous sections. However the difference is now with respect to the time at which the MTT forms. For the LTB, the shell at $r = 200$ forms the MTT at $t = 3215$ (see Fig. 4), whereas for the same choice of the density parameters, but with the choice of the parameter $a_1 = -(1/4)$, the same shell forms the MTT at $t = 1912$. The reason is that for these choices, the p_r is now nonzero and hence contributes to faster formation of the MTT (see Fig. 7). There also exist contributions from the p_t terms to the proper time of the observer falling along the shell.

(ii) For the exponential density profile given by the following form $\rho(r) = [m_0/8\pi r_0^3]\exp(-r/r_0)$, the situation is identical to the above case for the Gaussian profile. The time of formation of the MTT is lower than that obtained for the LTB case. For the LTB collapse, the MTT begins from the central singularity and develops as a dynamical horizon until approximately $r = 70$, and begins to resemble an isolated horizon (see Fig. 5). Here, the MTT formation and its spacelike nature are retained, although the time of formation of the isolated horizon are lowered at $t = 406$ (see Fig. 8) from that in the LTB case, which happens at $t = 660$.

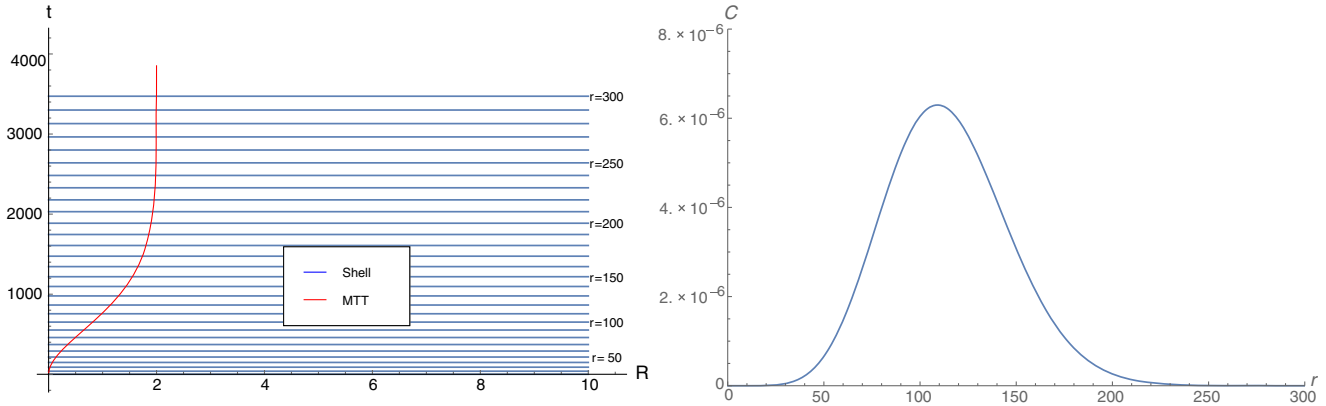

(a) (b)

FIG. 7. The graphs show the (a) formation of the MTT along with the shells and (b) values of C. The MTT begins from the center of the cloud and remains spacelike. The straight lines of the MTT in (a), after the shell at $r = 250$, represent the isolated horizon phase.

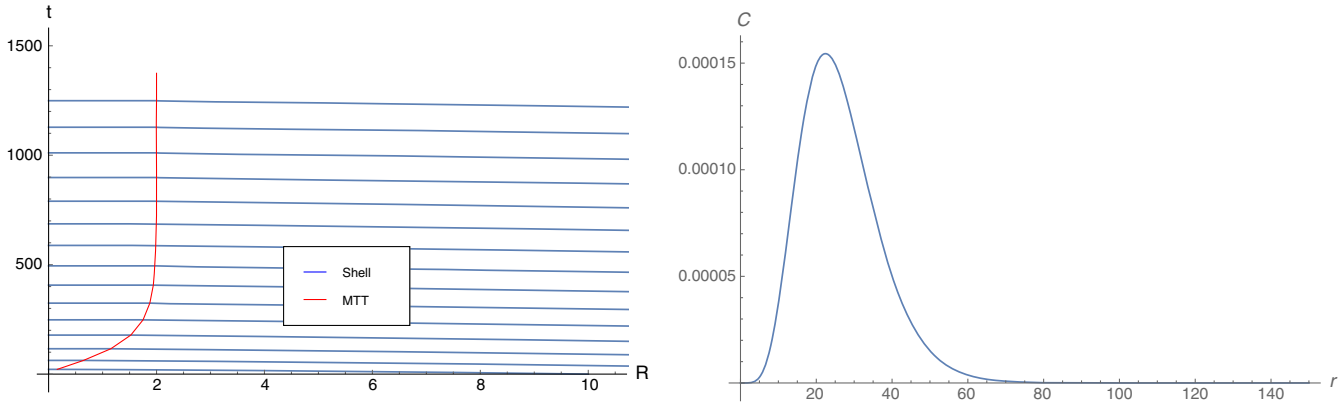

(a) (b)

FIG. 8. The formation of the MTT (a), and (b) values of C.

B. Time-dependent mass function

Let us consider the system in its full generality. The Einstein equations shall have all the following terms:

$$\rho = \frac{F'}{R^2 R'}; \qquad p_r = -\frac{\dot{F}}{R^2 \dot{R}} + (4/3)\eta\sigma + \zeta\theta, \tag{73}$$

$$\alpha' = \frac{2R'}{R}\frac{p_t - p_r + 2\eta\sigma}{\rho + p_r - (4/3)\eta\sigma - \zeta\theta} - \frac{p_r' - (4/3)\eta\sigma' - \zeta\theta'}{\rho + p_r - \frac{4}{3}\eta\sigma - \zeta\theta}, \tag{74}$$

$$(\dot{G}/G) = (2\alpha')(\dot{R}/R'); \qquad F(r,t) = R(1 - G + H). \tag{75}$$

Note that due to our generality, the Misner-Sharp mass function shall acquire time dependence. To solve this set of highly nonlinear coupled equations, we assume a set of constraints on the dynamical quantities: $p_r = k_r\rho$, $p_t = k_t\rho$, $\sigma = k_\sigma\rho$, and $\theta = k_\theta\rho$. By using these conditions, the solutions of the metric functions are

$$\exp(2\alpha) = \frac{R^{4a_1}}{\rho^{2a_2}}, \qquad \exp(2\beta) = \frac{R'^2}{1 + r^2 B(r,t)}, \tag{76}$$

where the parameters a_1 and a_2 are defined as $a_1 = [k_t - k_r + 2\eta k_\sigma]/[1 + k_r - (4/3)\eta k_\sigma - \zeta k_\theta]$ and $a_2 = [k_r - (4/3)\eta k_\sigma - \zeta k_\theta]/[1 + k_r - (4/3)\eta k_\sigma - \zeta k_\theta]$. The line element for this spacetime may thus be written as

$$ds^2 = -\frac{R(r,t)^{4a_1}}{\rho(r,t)^{2a_2}}dt^2 + \frac{R(r,t)'^2}{1 + r^2 B(r,t)}dr^2 + R(r,t)^2[d\theta^2 + \sin^2\theta d\phi^2]. \tag{77}$$

The equation of motion obtained from Eq. (75) is reduced to the form

$$\dot{R} = -R^{2a_1}\rho^{-a_2}\left[\frac{F(r,t)}{R} + r^2 B(r,t)\right]^{1/2}. \tag{78}$$

For an exact analytical solution, we introduce simplifications. Let us assume that the mass function $F(r,t)$, the metric function $B(r,t)$, and the density $\rho(r,t)$ are of the separable type,

$$F(r,t) = F_1(r)F_2(t), \qquad B(r,t) = B_1(r)B_2(t), \qquad \rho(r,t) = \rho_1(r)\rho_2(t), \tag{79}$$

where some of these functions are related, with the following conditions: $B_1(r) = k(r)/r^2$, $B_2(t) = -F_2(t) = -\rho_2(t)^{2a_2}$. Now, with the choice of the parametric form of $R(r,t) = [F_1(r)/k(r)]\cos^2(\eta/2)$, the equation of motion of the collapsing cloud (78) gives the following time curve:

$$dt = \frac{[F_1(r)\cos^2(\eta/2)]^{(1-2a_1)}\rho_1^{a_2}}{k(r)^{(3/2-2a_1)}}d\eta. \tag{80}$$

The solution of this equation which determines the motion of the collapsing cloud is given by complicated relations involving the hypergeometric functions

$$t = \frac{2F_1(r)^{1-2a_1}\rho_1(r)^{a_2}\cos(\eta/2)^{3-4a_1}}{(4a_1 - 3)k(r)^{3/2-2a_1}} \times {}_2F_1\left[\frac{1}{2}, \frac{3}{2} - 2a_1; \frac{5}{2} - 2a_1; \cos^2(\eta/2)\right] - \frac{2\sqrt{\pi}F_1(r)^{1-2a_1}\rho_1(r)^{a_2}}{(4a_1 - 3)k(r)^{3/2-2a_1}}\frac{\Gamma[5/2 - 2a_1]}{\Gamma[2 - 2a_1]}, \tag{81}$$

where ${}_2F_1(a,b;c;z)$ is the Gauss hypergeometric function, and $\Gamma(x)$ is the Gamma function. The boundary conditions are chosen such that collapse starts at $\eta = 0$, where $R(t_i, r) = [F(r)/k(r)]$ and $t = 0$. The cloud reaches the central singularity at $\eta = \pi$ where $R = 0$. In the t coordinates, the time of formation of central singularity is

$$t_s = \frac{2\sqrt{\pi}F_1(r)^{1-2a_1}\rho_1(r)^{a_2}}{(3 - 4a_1)k(r)^{3/2-2a_1}}\frac{\Gamma[5/2 - 2a_1]}{\Gamma[2 - 2a_1]}. \tag{82}$$

The dynamics of the marginally trapped surfaces (whether they are timelike, spacelike, or null) depends upon the sign of the expansion parameter C and is given by

$$C = \frac{1}{2\chi}\left[\frac{\rho + p_t - (4/3)\eta\sigma - \zeta\theta + (p_t - p_r)}{(4\pi/\mathcal{A}) - (1/2)\{\rho - \{p_t - (4/3)\eta\sigma - \zeta\theta + (p_t - p_r)\}\}}\right]. \tag{83}$$

1. Examples

(i) Gaussian: The density profile is the same as in Eq. (41). The assumed choices of parameters are $k_r = (1/2)$, $k_t = 1/4$, $\eta = 1/16$, $k_\sigma = 1/4$, $\zeta = (1/2)$, $k_\theta = (3/2)$ giving $a_1 = -0.3$ and $a_2 = -0.37$. The radial pressure has decreased, and hence, the time of formation of singularity or the spherically symmetric MTT is at a larger time compared to the LTB case (see Fig. 9). The MTT is still spacelike. Notice the shell labeled by $r = 200$. For the LTB case, it reached the isolated horizon at $t = 3215$, but here it

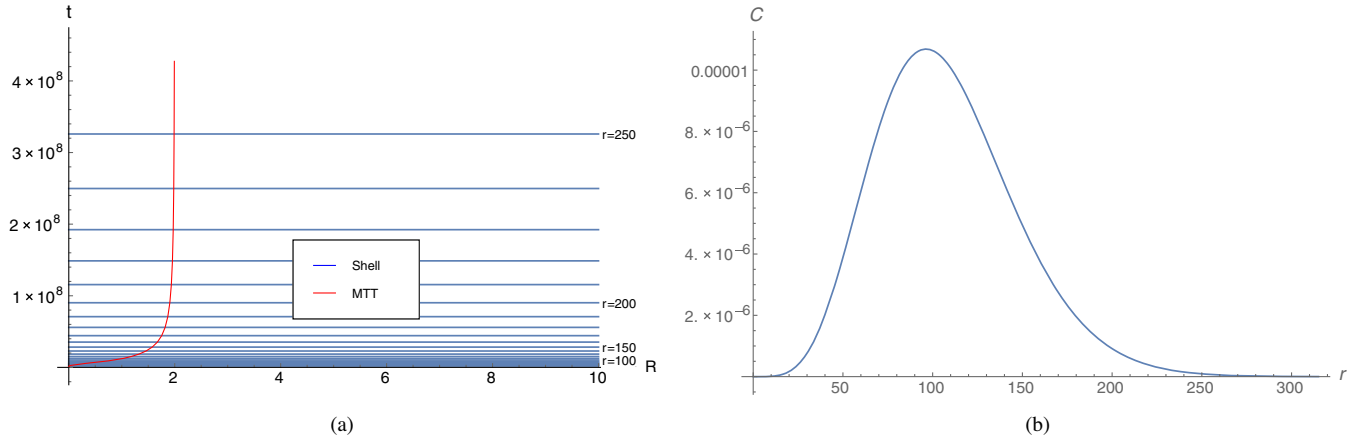

(a) (b)

FIG. 9. The graphs show the (a) formation of the MTT along with the shells, and (b) values of C. Again, note that the MTT begins from the center of the cloud and remains spacelike until it reaches the isolated horizon phase.

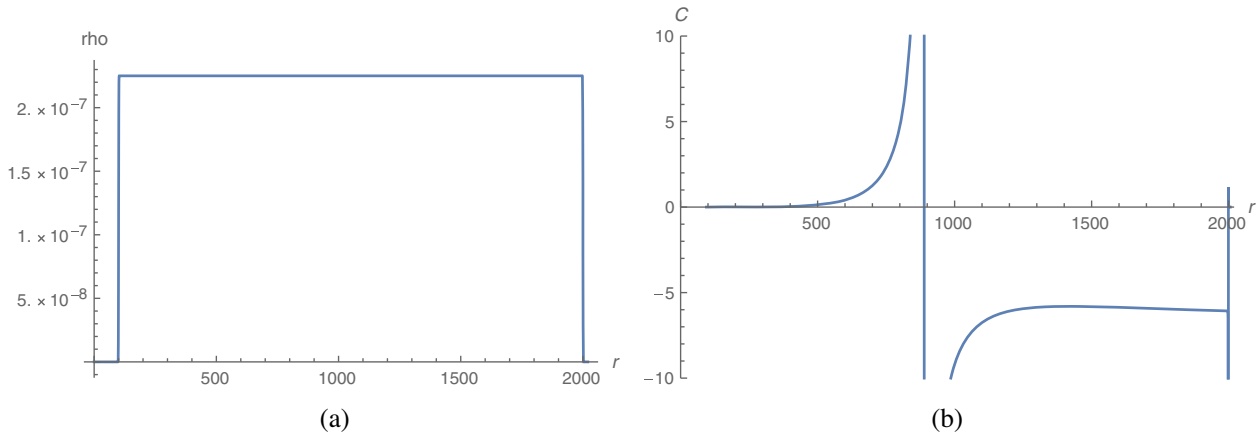

(a) (b)

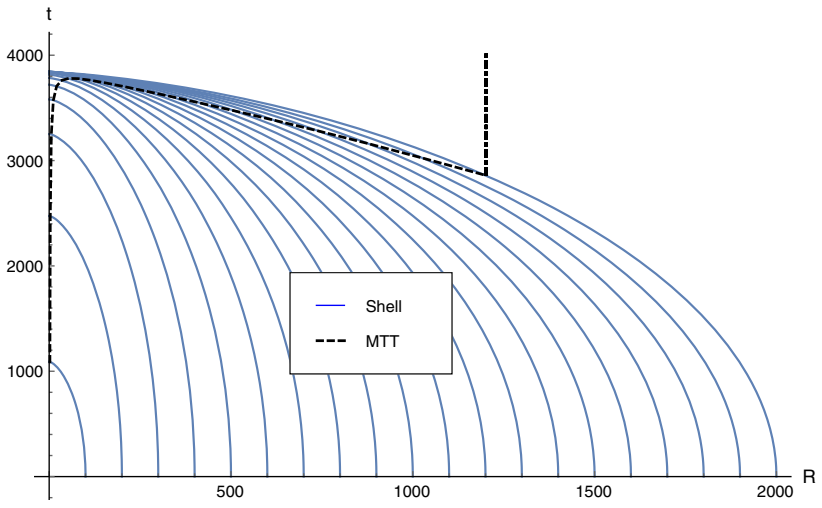

(c)

FIG. 10. The graphs show the (a) formation of MTT along with the shells, (b) values of C. The MTT is timelike. As seen from (c), it first forms at $t = 3000$ approximately, and bifurcates in one direction to reach the IH and in another direction to match the DH evolving out of the previous black hole.

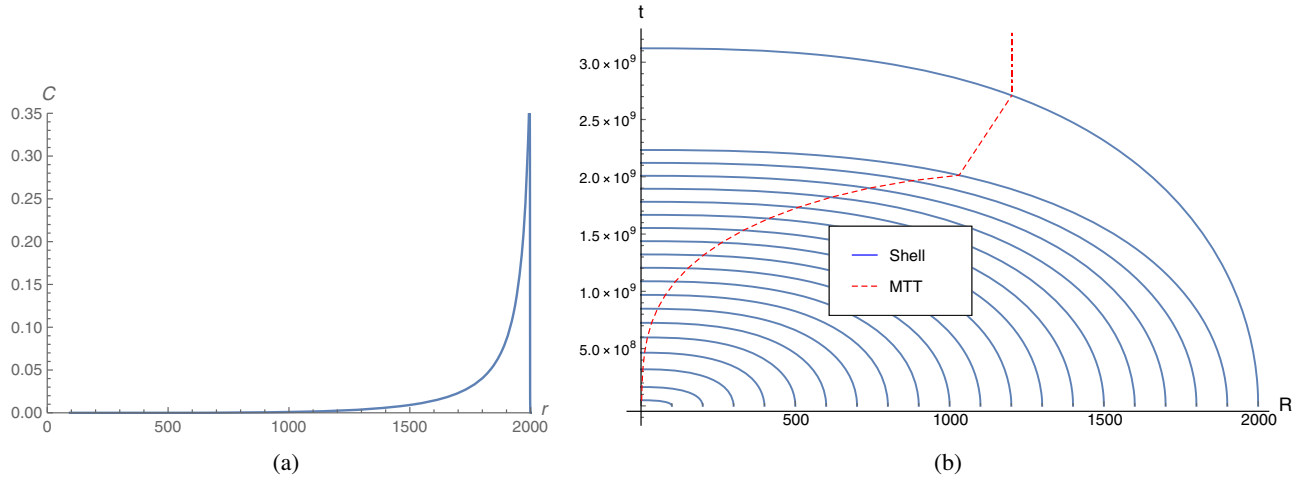

(a) (b)

FIG. 11. The graphs of (a) C and (b) MTT, for the same density profile as that of Fig. 10, but with different parameters. Here the MTT is spacelike.

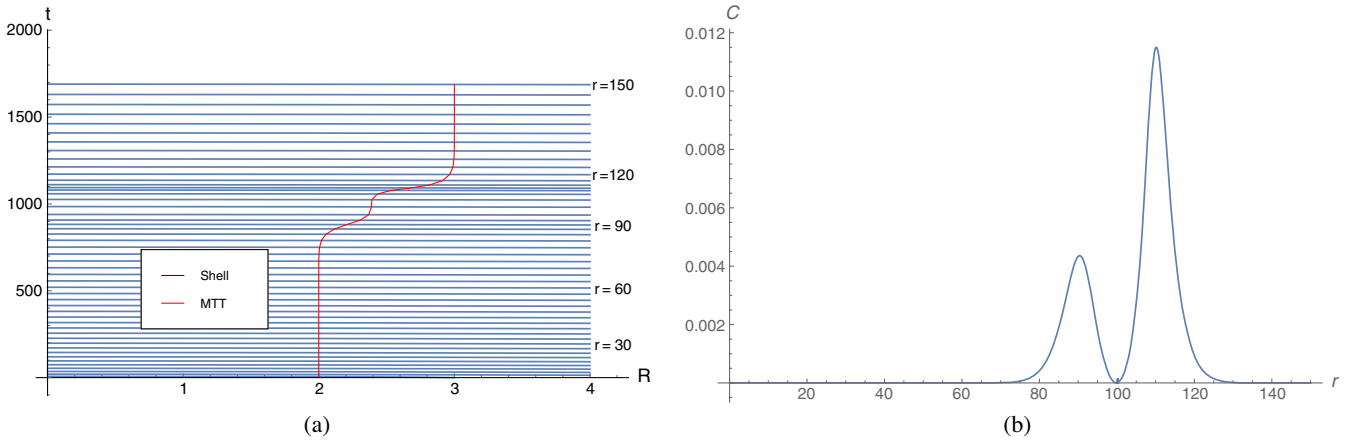

(a) (b)

FIG. 12. The graphs show the (a) formation of the MTT along with the shells, and (b) values of C. The MTT begins from the center of the cloud and remains spacelike. The straight lines of the MTT in (a) represent the isolated horizon phase.

happens at $t = 9 \times 10^7$, which is approximately a 10^3 factor higher. The reason is that with the choice of a time-dependent $F(r,t)$, the radial pressure has decreased considerably, and hence, the time of formation of the MTT for each shell also goes up. The nature of the formation of the MTT however remains identical.

(ii) Large shell: The nature of the formation of the MTT here is drastically different in nature from that described in the previous example. Here, we observe the formation of timelike MTTs. Here, for this more complicated collapse dynamics, the density profile generates a timelike tube. The MTT forms at about $r = 1800$ and bifurcates to reach the initial black holes. The timelike nature of the MTT is also confirmed from the values of C (Fig. 10). Here the choice of parameters is $k_r = (1/80)$, $k_t = 1/81$, $\eta = 1/16$, $k_\sigma = 1/20$, $\zeta = (1/12)$, $k_\theta = (1/8)$, giving $a_1 = 0.006$ and $a_2 = -0.002$. However, if the following choice of parameters is made, the MTT is spacelike: $k_r = 1/2$, $k_t = 1/10$, $\eta = 1/8$, $k_\sigma = 1/4$, $\zeta = 1/2$, $k_\theta = 3/2$, with $a_1 = -0.48$ and $a_2 = -0.41$ (see Fig. 11).

(iii) Two consecutive shells falling on a black hole: The density profile is same as in Eq. (43). Here, $k_r = (1/80)$, $k_t = 1/81$, $\eta = 1/16$, $k_\sigma = 1/20$, $\zeta = (1/12)$, $k_\theta = (1/8)$, giving $a_1 = 0.006$ and $a_2 = -0.002$ (see Fig. 12). The nature of the formation of the spherically symmetric MTT is identical to that described for the LTB model, although the time of formation of the MTT is not drastically delayed for these choices of parameter fields. Different choices of parameters change the time development of the MTT.

This study of spherically symmetric gravitational collapse of viscous matter using various mass profiles leads to a general understanding that the effects of viscosity, if not negligible, may lead to significant changes in the time of

the formation of horizons, as compared to the LTB models. Although this is a general result, the nature of the mass profile also plays a crucial role. Furthermore, the nature of the spherical MTT is also dependent on these viscosity parameters. Figures 10 and 11 show how the signature of MTT reverses due to change in the viscosity parameters. However, to classify these effects and to capture the interplay of viscosity parameters and the mass profile in this collapse process would require a much more detailed study.

VI. DISCUSSION

In this paper, we have developed analytical and numerical techniques to study the gravitational collapse of a large class of matter fields in Einstein's theory. The main focus has been to obtain the spherically symmetric trapped regions and locate the spherical marginally trapped surfaces for some general class of energy-momentum tensors, including fluids admitting bulk and shear viscosity. For the purpose of generality, we have included a brief discussion of homogeneous as well as inhomogeneous dust models. While the dust models have been studied earlier [3], a detailed study of the formation and time development of the EH and the spherical MTTs for a generic class of energy-momentum tensors, through analytical as well as numerical means, to our knowledge, has not been carried out in the literature. Our analytical methods focus on two specific aspects. The first aspect is to use the equations of gravitational collapse in the $R(r,t)-t$ coordinate system to trace the formation of the EH and the MTTs simultaneously with the collapse of the matter cloud. The use of the $R(r,t)$ is especially advantageous, since it is possible to track the horizons as well as the collapsing sphere at each moment. The second aspect is the development of numerical methods to locate the spherical trapped regions and marginally trapped surfaces for each of these matter fields. Through these numerical techniques, we have ascertained the validity of the analytical calculations as well as obtained a faithful representation of the general expectations about horizons during gravitational collapse. In particular, we have obtained the signature of the spherical MTTs during each of the collapse scenarios and a general conclusion may have been reached: The spherical MTTs inside the OSD matter cloud are timelike. The situation for LTB-like collapse is more complicated. Here, generically for $\dot{m}(r) > 0$, the MTTs are spacelike, and hence, all spherical MTTs are dynamical horizons which reach the isolated horizon phase in equilibrium. Thus, although the results are valid for spherically symmetric spacetimes, some general conclusions may possibly be drawn about the behavior of MTTs during the collapse.

While dealing with the viscous fluid, we have made some choices of viscosity parameters to restrict the values of the coefficients arising in the energy-momentum tensor. These parameters have been chosen because, for these range of values, we do not encounter shell crossing during gravitational collapse or have trapped surfaces at the beginning of the process. The numerical study of the evolution of spherical MTTs has been carried out for these cases only. We observe that, within the set of assumptions used here, it is possible to exploit the freedom of choice of the equation of state and the parameters to manipulate the nature as well as time of the formation of the MTT. Indeed, in the previous section, we have shown through examples, that alternate choices of initial data may lead to MTTs which are either timelike or spacelike. Furthermore, these choices also alter the time of formation of MTTs compared to the dust models, in the sense that MTT formation may be delayed or accelerated, compared to the dust models, by suitable choices in the fluid parameters. We believe a more extended study of these models may help in forming a general outlook on the time development of spherical MTSs during gravitational collapse.

In this paper, our attention has been on spherical MTTs, although nonspherical MTTs are also important. An important aspect of study of the MTTs or trapped surfaces involves identifying the boundary of a black hole region. The boundary of a trapped region is not known, although the Eardley conjecture claims that the event horizon of a black hole spacetime may be thought of as the boundary of (marginally outer) trapped surfaces [62]. Indeed, it has been shown that for Vaidya-type null collapse scenarios with mass $m(v)$ having upper bound, and accreting mass such that $\dot{m}(v) \geq 0$, the conjecture holds [63]. However, interestingly, it has also been found that given a trapping horizon, trapped surfaces (or parts of it) may extend outside the horizon and into the initial flat region of the Vaidya spacetime, and furthermore, nonspherically symmetric trapped surfaces may also extend outside the standard spherically symmetric trapping horizon [50,51,56,57]. So, the exact boundary of a trapped region is not clearly specifiable as of now. A related question is then the following: If the Eardley conjecture holds, does the event horizon allow a local description? One should expect from the global nature of the EH that this should not be so. Again for Vaidya-type collapse processes, it has been shown that trapped surfaces may be constructed which extend into the future and hence acquire nonlocal nature. Thus, the location and nature of the boundary of a strictly trapped region remains unknown. It seems that the process of further development needs numerical study of spherical as well as nonspherical MTTs in general relativity and in other alternate gravity theories to gain insight into the properties of MTTs. These issues will be addressed in future studies.

ACKNOWLEDGMENTS

The authors A. C. and A. G. are also supported by the DAE-BRNS Project No. 58/14/25/2019-BRNS. A. C. is

also supported by the DST-MATRICS scheme of the government of India through Grant No. MTR/2019/000916.

APPENDIX: JUNCTION CONDITIONS

The Israel-Darmois junction conditions provide a set of rules and boundary conditions which have been used in the previous sections. These boundary conditions are summarized below for some simple cases. In the following, we provide the junction conditions for a simple model: a $K = 0$ OSD model as the interior spacetime joined to an exterior Schwarzschild spacetime (denoted by $\mathcal{M}^-$) of mass M (denoted by $\mathcal{M}^+$) along a spacelike hypersurface Σ. Let us denote the coordinates on this surface as (τ, θ, ϕ). From $\mathcal{M}^-$, we can write down the surface Σ as $f_-(r,t) = r - r_b = 0$, and hence, the induced metric on Σ is

$$ds_-^2 = a(\tau)^2(-d\tau^2 + r_b^2 d\Omega^2). \tag{A1}$$

Note that the coordinates t and τ are related through the relation $dt/d\tau = a(\tau)$. From the point of view of the exterior spacetime, the hypersurface may be described by $r = R(\tau)$ and $t = T(\tau)$, with no change in the angular variables. The line element of the exterior manifold is then given by

$$ds_+^2 = -(Z\dot{T}^2 - Z^{-1}\dot{R}^2)d\tau^2 + R(\tau)^2(d\theta^2 + \sin^2\theta d\phi), \tag{A2}$$

where $Z = (1 - 2M/R)$. The matching of the metric immediately implies that the following two conditions hold:

$$R(\tau) = r_b a(\tau); \qquad a(\tau)^2 = [Z(dT/d\tau)^2 - Z^{-1}(dR/d\tau)^2]. \tag{A3}$$

The normal vector field n^a for $\mathcal{M}^-$ and the external spacetime $\mathcal{M}^+$ are given, respectively, by

$$n_a = a(\tau)(dr)_a, \quad n_a = -(dR/d\tau)(d\tau)_a + (dT/d\tau)(dr)_a. \tag{A4}$$

The velocity of observer on the cloud is also determined for these two patches of spacetime separately and are given by

$$\frac{dR(r_b,\tau)}{d\tau} = -a(\tau)[F(r_b)/R]^{1/2}, \tag{A5}$$

where the $-$ve sign is chosen to signify the collapse. The velocity as observed from the external coordinates is then $dR/dT = -(2M/R)(1 - 2M/R)$. Note also that the second of the metric matching conditions along with Eq. (A5) implies that $(dT/d\tau) = a/(1 - 2M/R)$. Using the normal vector fields, the extrinsic curvatures of the interior and the exterior spacetime may also be determined, and they give

$$K^-_{\tau\tau} = 0, \tag{A6}$$

$$K^+_{\tau\tau} = -\sqrt{\frac{2M}{R}}\left(1 - \frac{2M}{R}\right)\ddot{T} + \dot{a}\sqrt{\frac{2M}{R}} + \frac{4M^2a^2}{(1 - \frac{2M}{R})r_s^3}, \tag{A7}$$

$$K^-_{\theta\theta} = R\left[1 - \frac{F}{R} + \frac{2M}{R}\right]^{1/2}, \qquad K^+_{\theta\theta} = R. \tag{A8}$$

The $K_{\tau\tau}$ matching also gives us $(dT/d\tau) = a/(1 - 2M/R)$. The $K_{\theta\theta}$ matching gives us the equation

$$F(r_b) \equiv m r_b^3 = 2M. \tag{A9}$$

A similar exercise may also be carried out to join the interior spacetime created due to viscous fluid collapse given by Eq. (77), with the external Schwarzschild spacetime. In that case, the matching gives the following set of conditions. First, the $K_{\theta\theta}$ matching again gives $F(r_b, \tau) \equiv m(r_b, \tau) r_b^3 = 2M$. This matching, along with the mass function, leads to the equation $p_r = \zeta\theta + (4/3)\eta\sigma$, involving the radial pressure and viscosity terms at the boundary.

[1] S. W. Hawking and G. F. R. Ellis, *The Large Scale Structure of Spacetime* (Cambridge University Press, Cambridge, England, 1975).
[2] R. M. Wald, *General Relativity* (University of Chicago Press, Chicago, 1984).
[3] L. D. Landau and E. M. Lifshitz, *The Classical Theory of Fields* (Pergamon Press, New York, 1975).
[4] P. S. Joshi, *Gravitational Collapse and Spacetime Singularities* (Cambridge University Press, Cambridge, England, 2007).
[5] R. Penrose, Phys. Rev. Lett. **14**, 57 (1965).
[6] R. Penrose, Riv. Nuovo Cimento **1**, 252 (1969); Gen. Relativ. Gravit. **34**, 1141 (2002).
[7] S. Datt, Z. Phys. **108**, 314 (1938).

[8] J. R. Oppenheimer and H. Snyder, Phys. Rev. **56**, 455 (1939).
[9] G. Lemaitre, Gen. Relativ. Gravit. **29**, 641 (1997).
[10] R. C. Tolman, Proc. Natl. Acad. Sci. U.S. A. **20**, 169 (1934); Gen. Relativ. Gravit. **29**, 935 (1997).
[11] H. Bondi, Mon. Not. R. Astron. Soc. **107**, 410 (1947).
[12] C. W. Misner and D. H. Sharp, Phys. Rev. **136**, B571 (1964).
[13] W. C. Hernandez and C. W. Misner, Astrophys. J. **143**, 452 (1966).
[14] P. S. Joshi and D. Malafarina, Int. J. Mod. Phys. D **20**, 2641 (2011).
[15] R. Goswami and P. S. Joshi, Phys. Rev. D **76**, 084026 (2007).
[16] P. Yodzis, H. J. Seifert, and H. M. zum Hagen, Commun. Math. Phys. **34**, 135 (1973); **37**, 29 (1974).
[17] C. J. S. Clarke, *The Analysis of Spacetime Singularities* (Cambridge University Press, Cambridge, England, 1993).
[18] O. Dreyer, B. Krishnan, D. Shoemaker, and E. Schnetter, Phys. Rev. D **67**, 024018 (2003).
[19] A. Ashtekar and B. Krishnan, Living Rev. Relativity **7**, 10 (2004).
[20] I. Booth, Can. J. Phys. **83**, 1073 (2005).
[21] E. Schnetter, B. Krishnan, and F. Beyer, Phys. Rev. D **74**, 024028 (2006).
[22] S. A. Hayward, Phys. Rev. D **49**, 6467 (1994).
[23] A. Chatterjee, B. Chatterjee, and A. Ghosh, Phys. Rev. D **87**, 084051 (2013).
[24] A. Ashtekar, C. Beetle, O. Dreyer, S. Fairhurst, B. Krishnan, J. Lewandowski, and J. Wisniewski, Phys. Rev. Lett. **85**, 3564 (2000).
[25] A. Ashtekar, S. Fairhurst, and B. Krishnan, Phys. Rev. D **62**, 104025 (2000).
[26] A. Ashtekar and B. Krishnan, Phys. Rev. Lett. **89**, 261101 (2002).
[27] A. Ashtekar and B. Krishnan, Phys. Rev. D **68**, 104030 (2003).
[28] A. Ashtekar, J. Baez, A. Corichi, and K. Krasnov, Phys. Rev. Lett. **80**, 904 (1998).
[29] A. Chatterjee and A. Ghosh, Phys. Rev. D **91**, 064054 (2015).
[30] A. Chatterjee and A. Ghosh, Phys. Rev. D **92**, 044003 (2015).
[31] A. Ashtekar and G. J. Galloway, Adv. Theor. Math. Phys. **9**, 1 (2005).
[32] I. Booth, L. Brits, J. A. Gonzalez, and C. Van Den Broeck, Classical Quantum Gravity **23**, 413 (2006).
[33] A. M. Sherif, R. Goswami, and S. D. Maharaj, Classical Quantum Gravity **36**, 215001 (2019).
[34] A. M. Sherif, R. Goswami, and S. D. Maharaj, Int. J. Geom. Methods Mod. Phys. **17**, 2050097 (2020).
[35] S. L. Shapiro and S. A. Teukolsky, *Black Holes, White Dwarfs, and Neutron Stars: The Physics of Compact Objects* (Wiley, New York, 1983).
[36] T. W. Baumgarte and S. L. Shapiro, *Numerical Relativity* (Cambridge University Press, Cambridge, England, 2010).
[37] L. Rezzolla and O. Zanotti, *Relativistic Hydrodynamics* (Cambridge University Press, Cambridge, England, 2015).
[38] L. Herrera, A. Di Prisco, and E. Fuenmayor, Classical Quantum Gravity **20**, 1125 (2003).
[39] L. Herrera, A. Di Prisco, E. Fuenmayor, and O. Troconis, Int. J. Mod. Phys. D **18**, 129 (2009).
[40] P. Joshi, N. Dadhich, and R. Maartens, Phys. Rev. D **65**, 101501 (2002).
[41] R. Chan, L. Herrera, and N. O. Santos, Classical Quantum Gravity **9**, L133 (1992).
[42] R. Chan, Mon. Not. R. Astron. Soc. **316**, 588 (2000).
[43] Y. Kanai, M. Siino, and A. Hosoya, Prog. Theor. Phys. **125**, 1053 (2011).
[44] M. Blau, *Lectures on General Relativity* (2016), http://www.blau.itp.unibe.ch/Lecturenotes.html.
[45] I.Booth and S.Fairhurst, Phys. Rev. D **75**, 084019 (2007).
[46] L. Andersson, M. Mars, and W. Simon, Phys. Rev. Lett. **95**, 111102 (2005).
[47] L. Andersson, M. Mars, and W. Simon, Adv. Theor. Math. Phys. **12**, 853 (2008).
[48] I. Booth and J. Martin, Phys. Rev. D **82**, 124046 (2010).
[49] A. Krasinski and C. Hellaby, Phys. Rev. D **69**, 043502 (2004).
[50] I. Bengtsson and J. M. M. Senovilla, Phys. Rev. D **79**, 024027 (2009).
[51] I. Bengtsson and J. M. M. Senovilla, Phys. Rev. D **83**, 044012 (2011).
[52] I. Bengtsson, E. Jakobsson, and J. M. M. Senovilla, Phys. Rev. D **88**, 064012 (2013).
[53] I. Booth and D. W. Tian, Classical Quantum Gravity **30**, 145008 (2013).
[54] B. Creelman and I. Booth, Phys. Rev. D **95**, 124033 (2017).
[55] I. Booth, H. K. Kunduri, and A. O'Grady, Phys. Rev. D **96**, 024059 (2017).
[56] E. Schnetter and B. Krishnan, Phys. Rev. D **73**, 021502 (2006).
[57] A. B. Nielsen, M. Jasiulek, B. Krishnan, and E. Schnetter, Phys. Rev. D **83**, 124022 (2011).
[58] E. N. Glass, J. Math. Phys. (N.Y.) **20**, 1508 (1979).
[59] A. Banerjee and S. B. D. Chaoudhury, J. Math. Phys. (N.Y.) **30**, 867 (1989).
[60] A. K. Raychaudhuri, *Theoretical Cosmology* (Oxford University Press, New York, 1979).
[61] R. Misra and D. Srivastava, Phys. Rev. D **8**, 1653 (1973).
[62] D. M. Eardley, Phys. Rev. D **57**, 2299 (1998).
[63] I. Ben-Dov, Phys. Rev. D **75**, 064007 (2007).